University of Naples Federico II

Department of Electrical Engineering and Information Technology

Ph.D Course in Electrical Engineering – XXV cycle

PhD Thesis

POWER QUALITY MEASUREMENT METHODS AIMED AT DISTURBANCES DETECTION AND INSTRUMENTATION SUSCEPTIBILITY ASSESSMENT

Candidate
Ing. Giacomo Ianniello

Advisor
Prof Massimo D'Apuzzo

Assistant Advisor
Ing. Mauro D'Arco

Abstract

In this work several important aspects of power quality are discussed, and measurement methods aimed at disturbances detection are proposed.

A first aspect, investigated throughout laboratory tests, concerns the effects of poor power quality on measurement instrumentation. Susceptibility studies have been carried out considering the disturbances referred into standard CEI EN 50160. Controlled power quality disturbances have been injected in instrumentation and both reliability and accuracy issues have been checked in the test.

A second aspect taken into account is that related to the instrumentation needed for the analysis of the power quality. An original contribution that consists in the design and implementation of a distributed low-cost Arm-based network analyzer has been presented. The network analyzer is able to measure the power quality characteristics by each appliance. Furthermore, the proposed distributed analyzer includes a web server that allows to collect the statistics of each meter. A client can connect to the server to analyze meter group measurement results.

Several details related to suitable strategies to increase measurement resolution have also been considered. In particular a pre-processing scheme to enhance resolution of data acquisition systems mainly in presence of band-bass input signals has been investigated. This solution permits to acquire a seamless data stream with improved vertical resolution. An important feature is that this solution shows efficient in terms of hardware requirements and processing time.

Finally, since in power quality assessment harmonic analysis plays a key role, modeling and analysis of the functioning of power systems in time varying conditions has been studied with the purpose of understanding how harmonic analysis could be used effectively in these scenarios. In particular the power systems have been described trough simplified approaches by recognizing load conditions that can be considered stationary within limited time intervals. A data segmentation approach to distinguish the time intervals in which stationary load conditions can be recognized has been proposed and assessed.

Contents

Index of figures

Index of tables

Introduction

Electrical energy is a product and, like any other product, should satisfy the proper quality requirements. If electrical equipment is to operate correctly, it requires electrical energy to be supplied at a voltage that is within a specified range around the rated value. A significant part of the equipment in use today, especially electronic and computer devices, requires good power quality (PQ). However, the same equipment often causes distortion of the voltage supply in the installation, because of its non-linear characteristics, i.e. it draws a non-sinusoidal current with a sinusoidal supply voltage. The correct operation of electrical equipment requires a supply voltage that is as close as possible to the rated voltage. Even relatively small deviations from the rated value can cause erroneous operation of equipment, e.g. operation at reduced efficiency, or higher power consumption with additional losses. Sometimes prolonged deviations can cause operation of protection devices, resulting in outages. Of course, the correct operation of equipment also depends on many other factors, such as environmental conditions and proper selection and installation. Moreover, poor PQ often has large financial consequences to the affected customers (mainly to the industries with process plants). In extreme cases, poor PQ of the electric supply can cause financial losses to the network operators and the equipment manufacturers too [64]. It is estimated that losses caused by poor PQ cost EU industry and commerce about € 10 billion per annum [65]. So the investigation of the influence of supply voltage disturbances on equipment operation is a critical issue. A particular kind of devices, which plays an important role in the analysis of the state of an electrical system, is the instrumentation of measurement. Not all supply voltage disturbances cause outages of the equipment but some of them can only cause malfunctions. In particular, some disturbances injected in the measurement instrumentation power supply can cause measurement errors. So a susceptibility study of this particular equipment to power quality disturbances has been investigated in the chapter I.

Maintaining satisfactory PQ is a joint responsibility for the supplier and the electricity user. According to standard EN 50160 [4] the supplier is the party who provides electricity via a public distribution system, and the user or customer is the purchaser of electricity from a supplier. The user is entitled to receive a suitable quality of power from the supplier. In practice the level of PQ is a compromise between user and supplier. In this context electrical energy measurement plays a crucial role not only in commercial energy transactions but also in the estimation of energy balances in industries and in the performance evaluation of machines and energy systems, both traditional and innovative. With the integrated quality certification of the electrical services the possibility to stipulate contracts for quality for the customers has been introduced. This implies the fixation of an agreed level of quality ("Custom Power"). This requires on-line determination of energy flows and a corresponding level of quality. In order to reach this goal, digital signal processing techniques can be adopted; these techniques are commonly used in today's instrumentation world, both in the scientific and industrial fields. however electrical measurements on power systems, in non-sinusoidal conditions, require suitable instrumentation supported by theoretically correct methods. In chapter II the power quality measurement methods are discussed analyzing both standards produced by the international committees and the instruments aimed to this kind of measurements such as the *network analyzers*. Then aspects of implementation of a distributed low-cost Arm-based network analyzer are proposed. The network analyzer is able to measure the power quality characteristics by each appliance. Furthermore, the proposed distributed analyzer includes a web server that allows to collect the statistics of each meter. A client can connect to the server to analyze meter group measurement results. The network analyzers as well as the modern instrumentation of measurement are based on the digital processing of physical-world signals that requires their conversion into digital format which can be carried out by analog to digital converters (ADC). So Several details related to suitable strategies to increase measurement resolution have been considered. In particular a pre-processing scheme to enhance resolution of data acquisition

systems mainly in presence of band-bass input signals has been investigated in the chapter III. This solution permits to acquire a seamless data stream with improved vertical resolution. An important feature is that this solution shows efficient in terms of hardware requirements and processing time .

The results of PQ measurement give information about the state of the disturbances existing on the electrical power network. This information can be used in different ways: (i) to observe the power network status; (ii) to provide information about the harmonic pollution; (iii) to prevent equipment failure.

An useful tool to reach these purposes is the electrical system modeling. For designers and technicians involved in design and maintenance of electrical power systems the definition of suitable models represents a very important issue. Actually, the use of models is precious for establishing proper control strategies, in order to prevent and avoid faults and energy losses, as well as for balancing the loads in three-phase systems. However modeling, control and management operations require the deployment of measurement methods capable of characterizing the power systems. Methods that are largely employed rely on the assumption of stationary load conditions, and are mainly based on harmonic analysis. Unfortunately, in a number of cases, time varying effects, which result in time varying harmonics, cannot be neglected. The major cause of the time variation is the asynchronous connection and disconnection of the electrical facilities. Nonetheless several loads can be inherently time varying [41],[42].

The analysis of time-varying harmonics represents a tough issue, which requires the evaluation of a time dependent spectrum by means of time frequency representations, or else the deployment of statistical and probabilistic methods [43-48]. However these methods require high computational burden. To cope with the time varying conditions of the system, the models proposed in the literature try to recognize within limited time intervals stationary load conditions [49-50]; a specific description of the system is therefore provided for each time interval. The recognition of different load conditions mainly relies on data segmentation techniques [51]. A new data segmentation approach to distinguish and separate

different load conditions in a power system is proposed and shown in the chapter IV.

I. Power quality in electrical power systems and its effects on equipment: instrumentation susceptibility assessment

In this chapter some of definitions of the term *power quality* are discussed. Then some effects of power quality disturbances on the equipment are reported, and finally susceptibility studies of measuring instruments have been carried out considering power quality disturbances. Controlled power quality disturbances have been injected in instrumentation and both reliability and accuracy issues have been checked in the tests.

1. Definition of Power Quality

Various sources give different and sometimes conflicting definitions of power quality. The Institute of Electrical and Electronics Engineers (IEEE) dictionary [55, page 807] states that "power quality is the concept of powering and grounding sensitive equipment in a matter that is suitable to the operation of that equipment." One could, for example, infer from this definition that harmonic current distortion is only a power quality issue if it affects sensitive equipment. Another limitation of this definition is that the concept cannot be applied anywhere else than toward equipment performance.

The International Electrotechnical Commission (IEC) definition of power quality, as in IEC 61000-4-30 [7], is as follows: "Characteristics of the electricity at a given point on an electrical system, evaluated against a set of reference technical parameters." This definition of power quality is related not to the performance of equipment but to the possibility of measuring and quantifying the performance of the power system.

As shown in Fig. I-1, according to Cigree, the term power quality is connected to two aspects:

- **Continuity of voltage**: availability of electricity;
- **Quality of voltage**: the presence of low-frequency noise that can propagate through the grid.

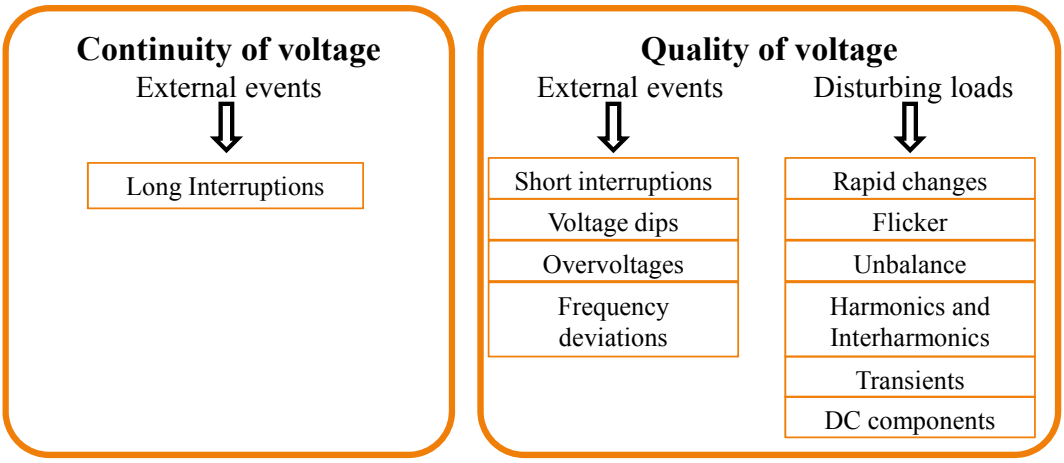

Fig. I-1: classification of power quality disturbances

The contract stipulated between the distribution company and the consumer reports the details of tolerances and limits of acceptability of the service. Today, with the spread of distributed generation, the consumer can also be producer, so it has to respect the same constraints imposed by the distributing companies.

The distributed generation has changed the functioning of electrical networks, now there are bidirectional flows of energy. So it needs to provide better management of flows. In this context the so-called "Smart Grid" play a crucial role. The smart grid is an information network that manages the electricity distribution network in an intelligent way. In particular, it provides an optimized management of energy flows in order to avoid waste of energy: in practice, any surplus of energy present in some areas can be redistributed, dynamically and in real time, to other lacking areas.

2. Effects of power quality disturbances on equipment.

Now-a-days the customers use large number of devices at their installations that consist of power electronics. The residential customers use different domestic appliances such as televisions (TV), video cassette recorders (VCR), microwave ovens, personal computers (PC), heating-ventilation-air conditioning equipment (HVAC), dishwashers, dryers etc. The business and office equipment include workstations, PCs, copiers, printers, lighting etc. On the other hand, the industrial

customers use programmable logic controllers (PLC), automation and data processors, variable speed drives (VSD), soft starters, inverters, computerized numerical control (CNC) tools and so on. Presently, many customers use compact fluorescent lamps (CFL) for lighting their installations. Many of these devices are quite sensitive to PQ disturbances. Case studies and surveys in different countries around the world have been done to estimate the impacts of poor PQ to the customers. However, until now, only few cases are surveyed to analyze the technical and non-technical inconveniences of poor PQ to the network operators.

From various surveys, it was generally noticed that industries are vulnerable to long and short interruptions (that are considered as 'reliability issues' in the power system analysis). Voltage dip is the main PQ problem for the semiconductor and continuous manufacturing industries, and also to the hotels and telecom sectors. Harmonic problems are perceived mainly by the commercial organizations and service sectors such as banks, retail, telecom etc. Another PQ problem that draws high attention is the presence of transients and surges at the customer's installation. In 2001, the Leonardo Power Quality Initiative (LPQI) surveyed in eight countries of the European Union (EU) [66] and declared that the customers report a complaint to the network operators when they suffer one of the inconveniences as shown in Table I-1 at their sites due to poor PQ of the electric supply.

In 2008, another report was published by the LPQI in which PQ survey was conducted among the customers of the EU-25 countries [67]. It was reported that loss of synchronization of processing equipment is an acute problem in the industries (mainly for the continuous manufacturing process plants). Lock ups of computers and switching equipment tripping are the second largest problem for industries. For the service and transport sectors, circuit breaker tripping and data loss have been identified as the main problems caused by poor PQ. It was noticed that main sources of PQ disturbances in the industries are the motor driven system and static converters. In contrast, PQ problems in the service sectors are mainly originated from various electronic equipment.

Perceived inconvenience	*Affected devices*	*Reported PQ problem*
Computer lock-ups and data loss	IT equipment (that are sensitive to change in voltage signal)	Presence of earth leakage current causing small voltage drops in earth conductors
Loss of synchronization in processing equipment	Sensitive measurements of process control equipment	Severe harmonic distortion creating additional zero-crossings within a cycle of the sine wave.
Computer, electronics equipment damage	Electronic devices like computer, DVD player etc.	Lightning or a switching surge
Lights flicker, blink or dimming	Flickering, blinking or dimming of lighting devices, and other visual screens	Fast voltage changes leading to visible light flicker
Malfunctioning of motors and process devices. Extra heating, decreased operational efficiency and premature aging of the equipment	Motors and process devices	Presence of voltage and current harmonics in the power supply
Nuisance tripping of protective devices	Relays, circuit breakers and contactors	Distorted voltage waveform because of voltage dip
Noise interference to telecommunication lines	Telecommunication system	Electrical noise causing interference signals

Table I-1: Customer's reported complaints in EU-8 as per LPQI survey

Fig. I-2 illustrates the LPQI survey results that indicate the frequency of different PQ consequences to the industries and the service and transport sectors as a percentage of cases analyzed.

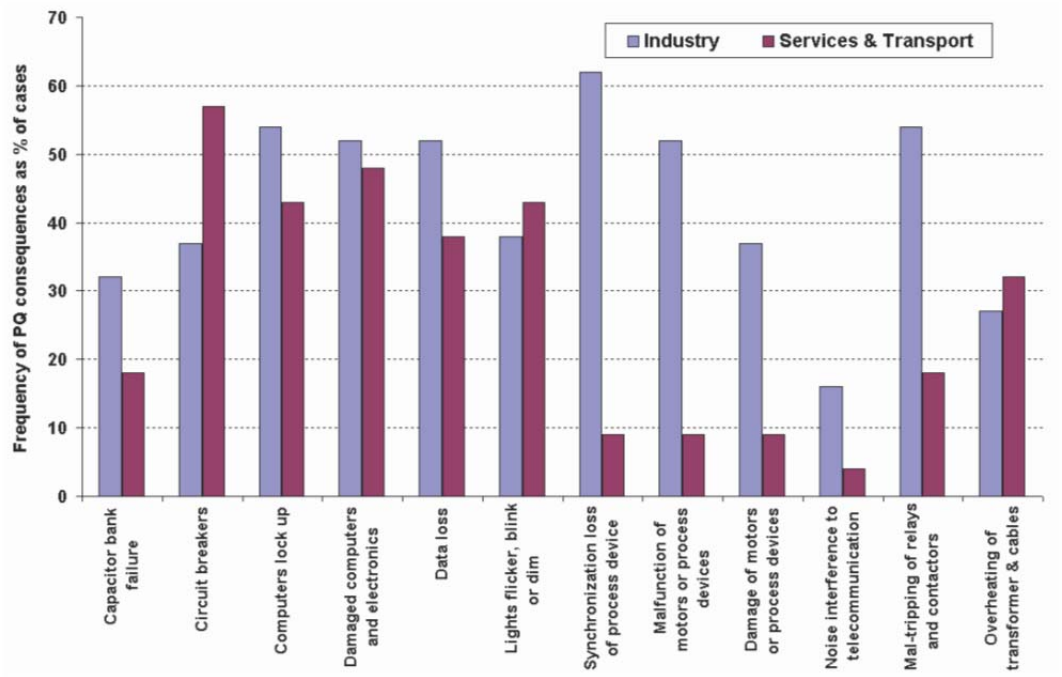

Fig. I-2: Consequences of poor PQ as experienced by the customers

Fig. I-3 shows the survey results [67] of the devices that mostly get affected by one of the PQ problems in different installations in the EU-25 countries. It shows that electronic equipment are the most vulnerable to PQ disturbances both in the industries as well as in the service and transport sectors. In 2000, the EPRI and CEIDS consortium conducted a PQ survey [68] among the industrial customers in the USA. It was declared that the most affected devices in the industries because of poor PQ are computers and microprocessor based devices (43%), variable speed drives (13%), lighting equipment (8%), motors (5%), relays (1%) and other equipment (30%). The 4th benchmarking report [69] of the European Regulators also gave an overview of PQ related costs in different countries of the world.

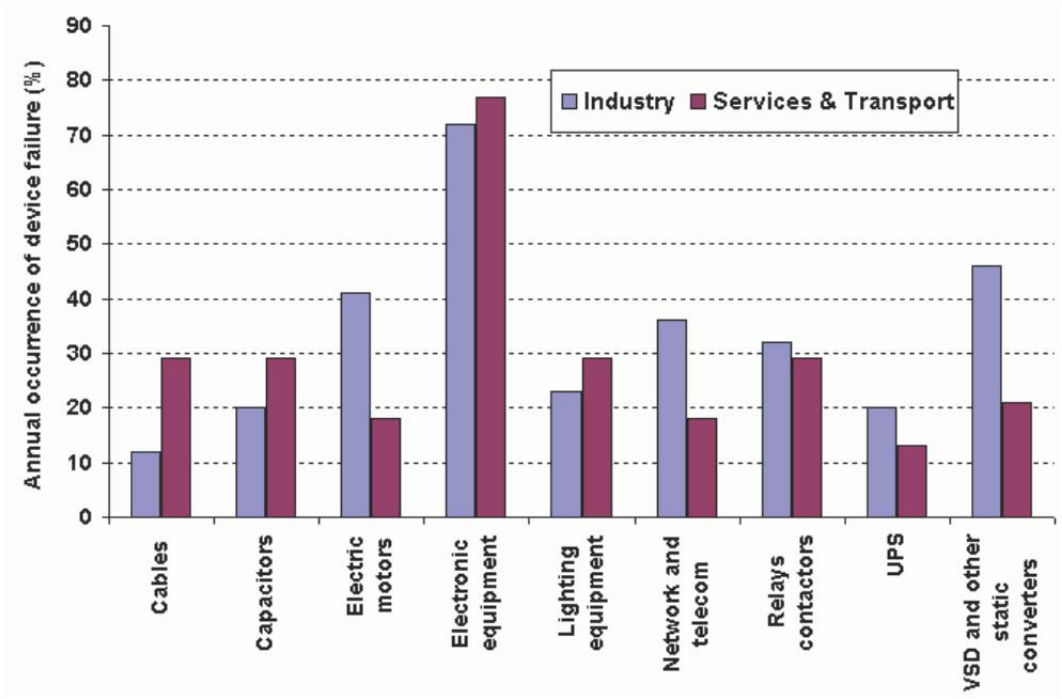

Fig. I-3: Equipment affected by PQ problems in different sectors

In Fig. I-4 an example of a three-phase unbalance is shown. In the figure are shown the RMS values of the neutral current (yellow trace) and the three-phase currents (blue, green and red traces) of the power supply of a mechanic's workshop. It can be noted that the RMS value of the neutral current is comparable with the RMS values of the current in the three phases. The unbalance in the observed system is caused mainly by harmonic distortion caused by the operation of the industrial welders (Fig. I-5). This effect can cause an unexpected action of protection devices.

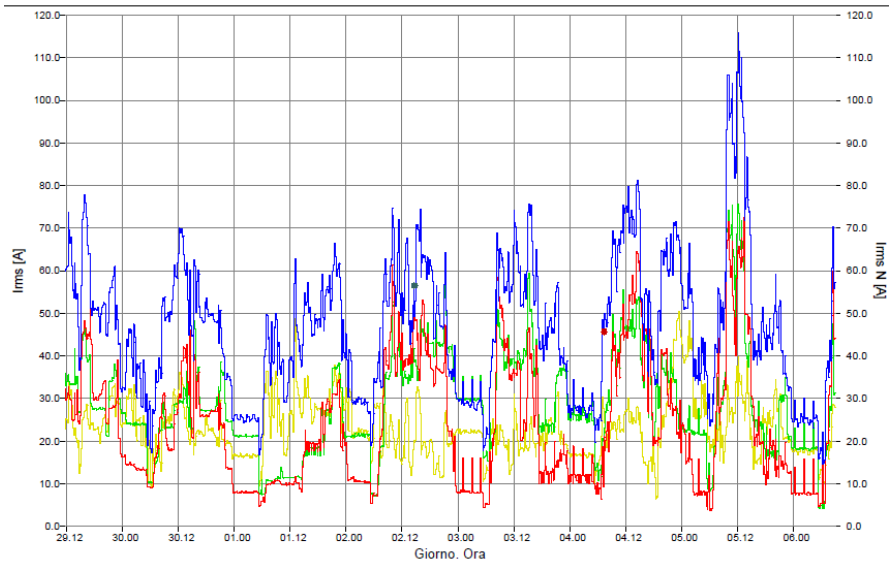

Fig. I-4: Effect of the unbalance: the RMS value of the neutral current (yellow trace) is comparable with the RMS values of the current in the three phases.

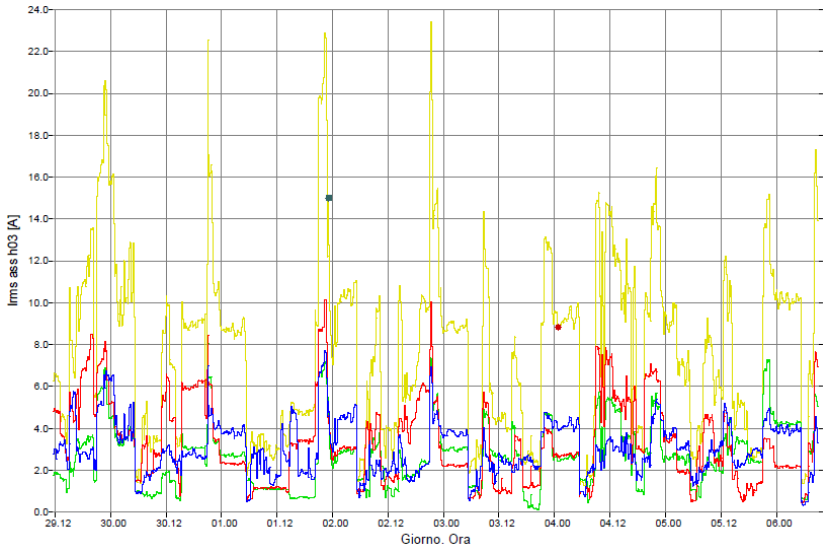

Fig. I-5: The unbalance in the observed system is caused mainly by harmonic distortion

The poor power quality has also costs: in Fig. I-6 are shown the costs of unexpected voltage interruptions in several Swedish industrial sectors. The study was carried out by the CESI. In the figure it can be notice that the poor power quality may also have up to 100 $ per interrupted kW.

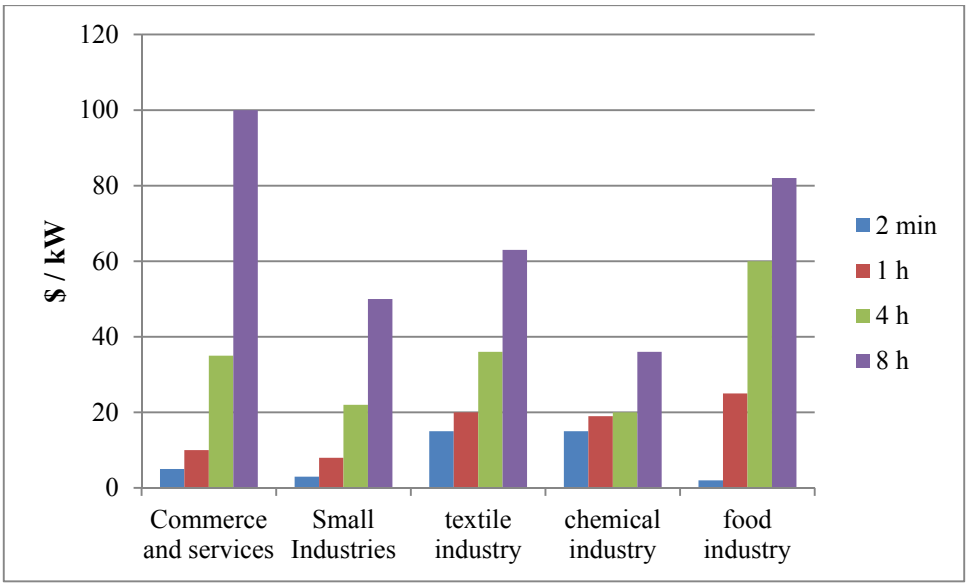

Fig. I-6: CESI report: costs of unexpected voltage interruptions in several Swedish industrial sectors

3. Susceptibility study of instrumentation of measurement to power quality disturbances

A particular kind of devices, which plays an important role in the analysis of the state of an electrical system, is the instrumentation of measurement.

The problem could bypass if each instrument was equipped with its own power supply: generally all instruments for measuring power quality disturbances are equipped with a backup battery that make the instrument insensitive to the poor power quality. However not all disturbances cause out of service of the equipment but some of them only cause malfunctions. In particular, some disturbances injected in the measurement instrumentation power supply can cause measurement errors (Fig. I-7).

Thus a susceptibility study of this particular equipment to power quality disturbances has been carried out: in particular controlled power quality disturbances have been injected in instrumentation and both reliability and accuracy issues have been checked in the tests.

Fig. I-7: effect of power quality disturbances on instrumentation of measurement

A. Instrumentation of Measurement under test

Three digital Multimeter have been tested:

a) Keithley 2001: 7½-Digit DMM w/ 8k Memory High Performance Multimeter; 1 Hz - 15 MHz frequency range; 200 mV – 1000 V voltage range;
b) Fluke 8845A Digital Multimeter, 6½ Digit; 10000 measurements storing in internal memory; 1 Hz - 300 kHz frequency range with 1 s, 100 ms and 10 ms programmable gate time; 100 mV – 1000 V voltage range.
c) Agilent 34401: 6 ½ Digit Multimeter

Every multimeter is based on a multi-ramp integrating voltmeter.

B. PQ Disturbances

Disturbances referred into standard CEI EN 50160 have been treated. The standard defines the main characteristics of the supply voltage for public MV/LV distribution users in nominal operating conditions. It reports the limits in which remain the characteristics of supply voltage in nominal operating conditions. Disturbances treated into standard have been injected in instrumentation power supply. Because the instrumentation of measurement under study is supplied with V_{RMS} = 230/120 [V], only LV characteristics and constraints have been taken into account. The Pacific Power Source, model AMX 360 has been used to generate the PQ disturbances.

Following the disturbances that have been injected in the instrumentation power supply, are listed:

1. **Voltage Magnitude Variation**:
   a. $U_{Supply} = U_n + 10\% \cdot U_n = 253V$;
   b. $U_{Supply} = U_n - 10\% \cdot U_n = 213V$;
2. **Supply Voltage Dips:**
   a. $\Delta U = 20\% \cdot U_n \quad \Delta t = (0.5; 1)s$
   b. $\Delta U = 30\% \cdot U_n \quad \Delta t = (0.5; 1)s$
   c. $\Delta U = 40\% \cdot U_n \quad \Delta t = (0.5; 1)s$
3. **Short interruptions of supply voltage:**

   These disturbances have not been treated in this study because they certainly would have caused the shutdown of instrumentation, then a measurement error of 100%.
4. **Long interruptions of supply voltage:**

   These disturbances have not been treated in this study because they certainly would have caused the shutdown of instrumentation, then a measurement error of 100%.
5. **Temporary, Power Frequency Overvoltages**: this disturbance has already been treated in the first disturbance listed above: Voltage Magnitude Variation.
6. **Supply Voltage Unbalance**: this disturbance has not been treated in this study because the instrumentation under tests is a single-phase load.

C. Tests Planning

The test bench block diagram is shown in the Fig. I-8:

The nominal supply voltage and frequency values of the instrumentation of measurement are 230/120V, 50/60Hz.

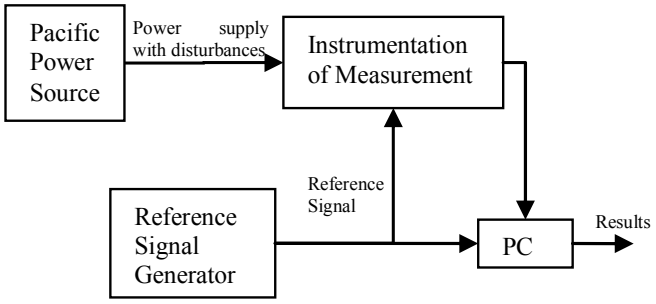

Fig. I-8: Test Bench Block Diagram

In the tests, the aforementioned disturbances, one-by-one, have been injected in the instruments power supply. Then DC voltage measurements have been carried out by the instruments: two dc voltages have been measured, first to half instrumentation full-scale, latter to instrumentation full-scale.

Three different integration times have been set for each instrument and for each test:

- Fast;
- Medium;
- Hi-Accuracy;

for each instrument the max configurable resolution, according to integration time chosen, has been set.

To control every instrument (Pacific Power Source, Multimeters, reference signal generator) the standard GPIB (IEEE 488) bus has been used.

The measurement procedure employed in this research activity is next.

DC Voltage Measurement Tests have been carried out for each instrument, for each integration time, for both voltage levels chosen above, following the flow chart shown in the Fig. I-9.

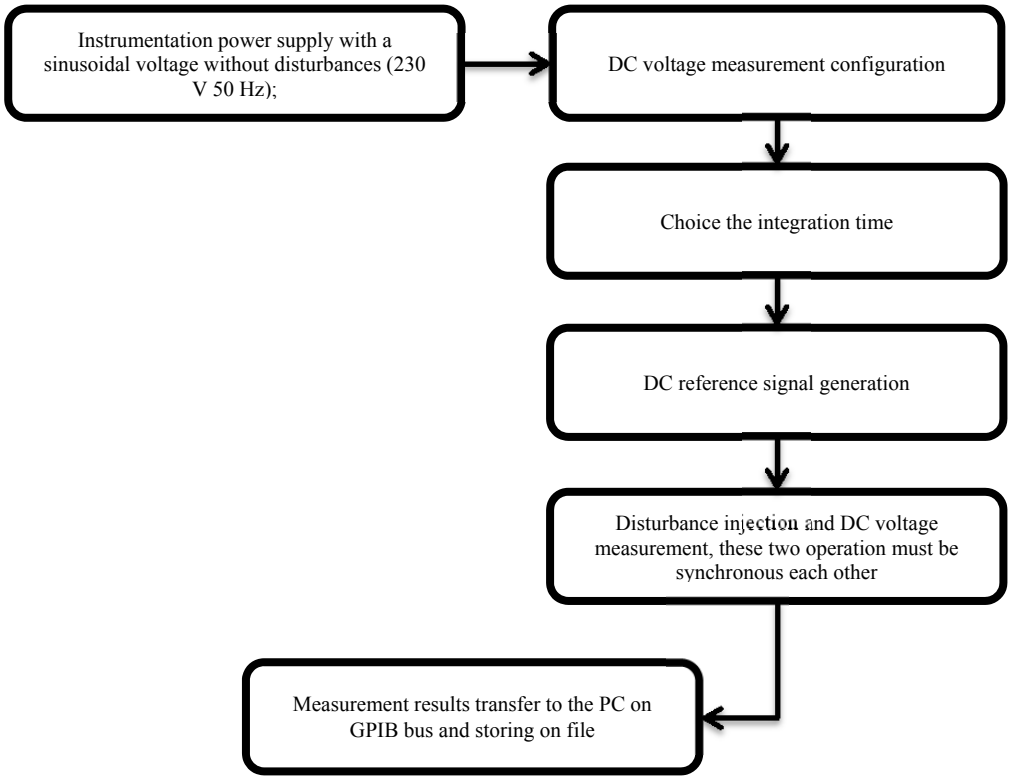

Fig. I-9: measurement procedure employed in this research activity

D. Storing Test Results

Files.

A text file (*.txt) for every test has been created to store measurement results. The files have been named:

"*Test_<instrument>_<integration time>_<Measurement>_<Measurement characteristic>_<Disturbance>".*

According to the integration time chosen, one of the following members has been inserted in the "integration time" field,: "*F"* (Fast); "*M"* (Medium); "*S"* (Slow).

According to the voltage level chosen, one of the following members has been inserted in "measurement characteristic" field: "*MFS"* (half full-scale), "*FS"* (full-scale).

The members inserted in the Disturbance field have been listed in Table I-2.

The last value stored in every file is the reference measurement set into reference generator.

Folders.

A folder named "*Measurement_Results_<Instrument>"* has been created for each instrument under test.

One subfolder, named *"Voltage_Measurement"* has been created inside the "*Measurement_Results_<Instrument>"* folder.

Table I-2: Disturbance Field Structure

Disturbance	Voltage magnitude (ΔU)	length (Δt) [s]	Member of <disturbance> field
Voltage Magnitude Variation			SupplyV
	U_n + 10% U_n	∞	V+10
	U_n - 10% U_n	∞	V-10
Voltage dip			Dip
	20 % U_n		V20
	30 % U_n		V30
	40 % U_n		V40
		0.5	T05
		1	T1

Two subfolders, named "*MFS"* and "*FS"* (relatively to the voltage level chosen), have been created inside the "*Voltage_Measurement"* subfolder.

Three subfolders, named *"Fast"*, *"Medium"* and *"Slow"* (relatively to the integration times chosen) have been created inside the *"MFS"* and *"FS"* subfolders.

Finally a folder named *"Sensibility_Test_Results"* has been created. This is the main folder containing the aforementioned subfolders.

E. Results

In the Fig. I-10 are shown the measurement results with supply voltage dips with $\Delta U = (20, 30, 40)\% \cdot U_n$ and duration $\Delta t = 0.5s$. The voltmeters have been

programmed in *fast acquisition mode* $(gate\,time = 2ms)$. The figure shows that during the voltage dip, the voltmeter measures a variable voltage instead of a constant one. The measurement error is proportional to the depth of the voltage dip.

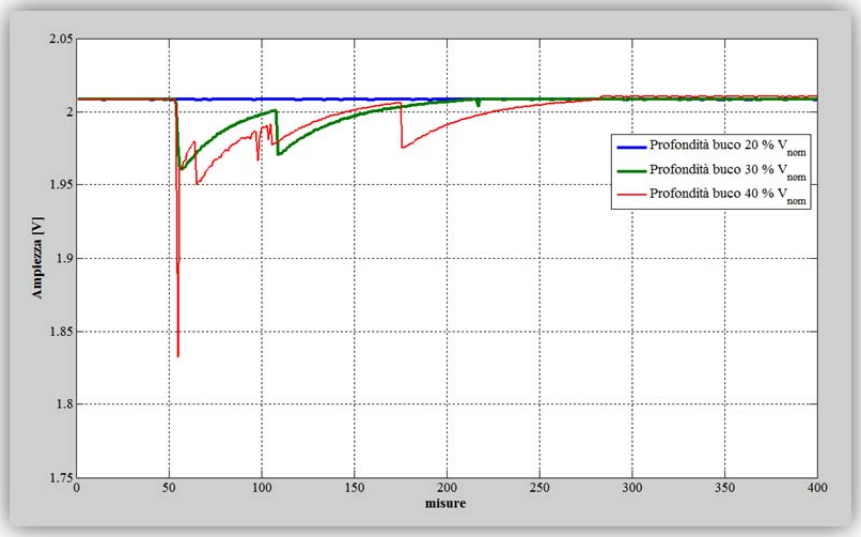

Fig. I-10: Gate time=2ms, Dip duration: 0,5 s

In the Fig. I-11 are shown the measurement results with supply voltage dips with $\Delta U = (20, 30, 40)\% \cdot U_n$ and duration $\Delta t = 1s$. The voltmeters have been programmed in *fast acquisition mode* $(gate\,time = 2ms)$. Since the voltage dip duration is greater than before, also the measurement errors are greater.

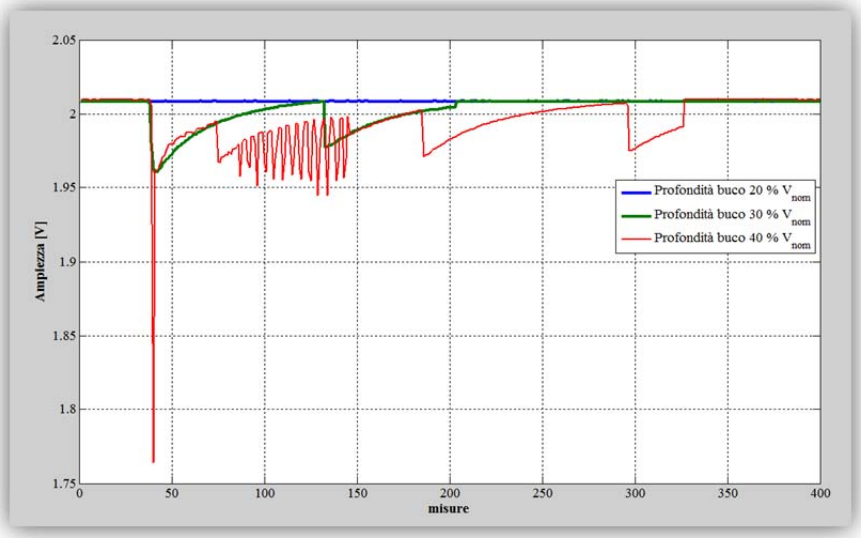

Fig. I-11: Gate time=2ms, Dip duration: 1 s

In the Fig. I-12 and Fig. I-13 are shown the measurement results with supply voltage dips with $\Delta U = (20, 30, 40)\% \cdot U_n$ and durations $\Delta t = (0.5, 1)s$ respectively. In this case the voltmeters have been programmed in *slow acquisition mode* $(gate\,time = 200ms)$. Also increasing the gate time, the voltmeter provides incorrect results of measurement during the voltage dips.

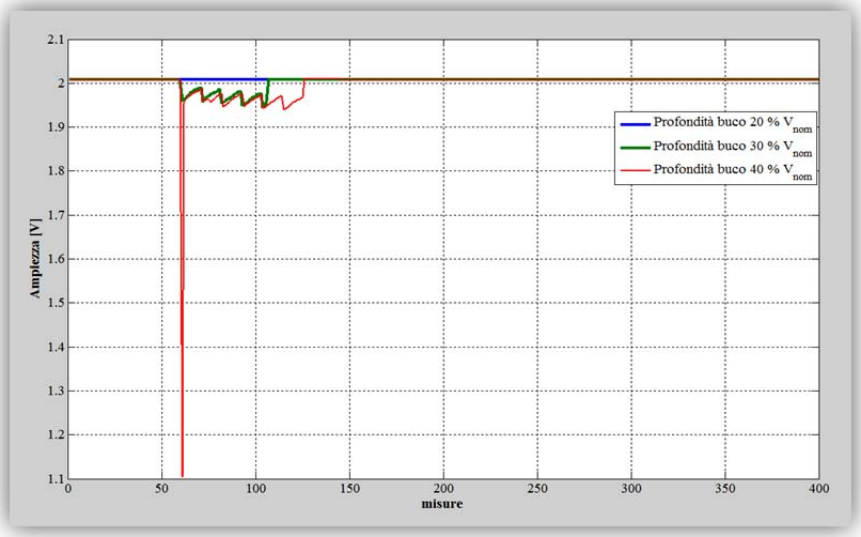

Fig. I-12: Gate time=200ms, Dip duration: 0,5 s

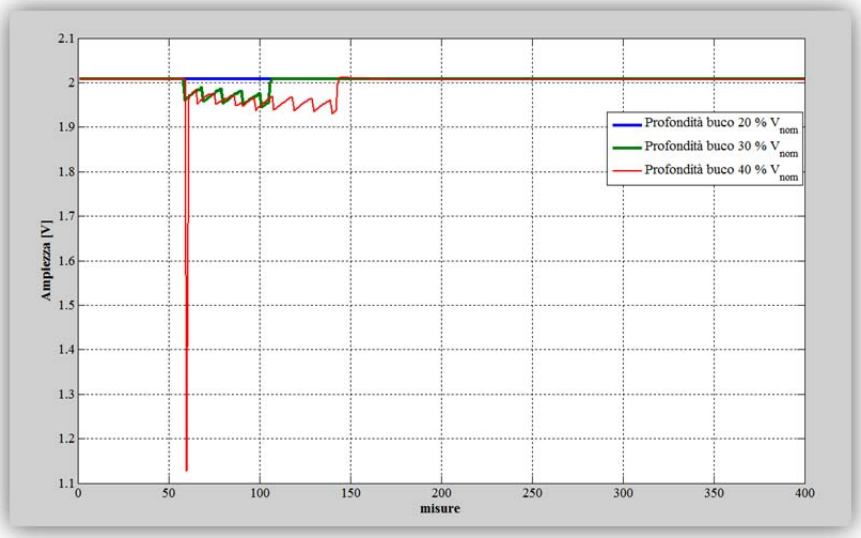

Fig. I-13: Gate time=200ms, Dip duration: 1s

Finally in the Fig. I-14 and Fig. I-15 are shown the mean error variations as a function of the voltage depth and the acquisition mode. The maximum errors achieved is of 1% corresponding to $\Delta U = 40\% \cdot U_n$; voltage dip duration $\Delta t = 1s$ and when the voltmeter has been programmed in *fast acquisition mode* $\left(gate\,time = 2ms\right)$, as shown in Fig. I-15.

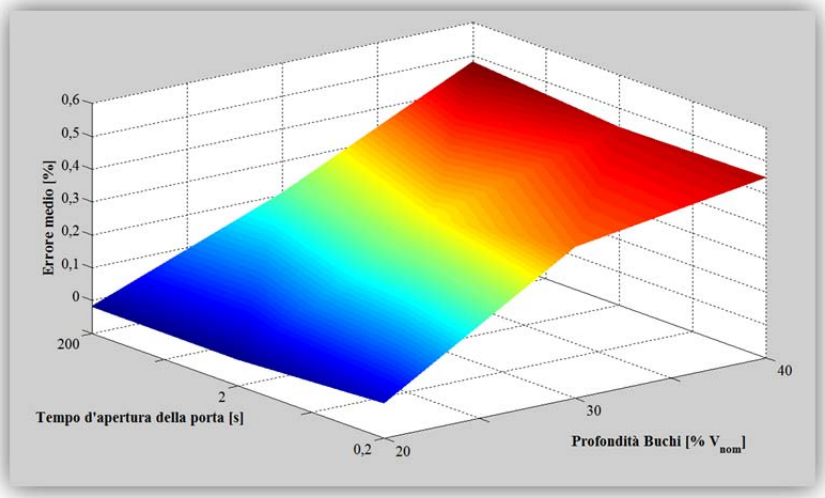

Fig. I-14: Mean error vs. voltage dip depth and gate time; voltage dip duration: 0,5 s

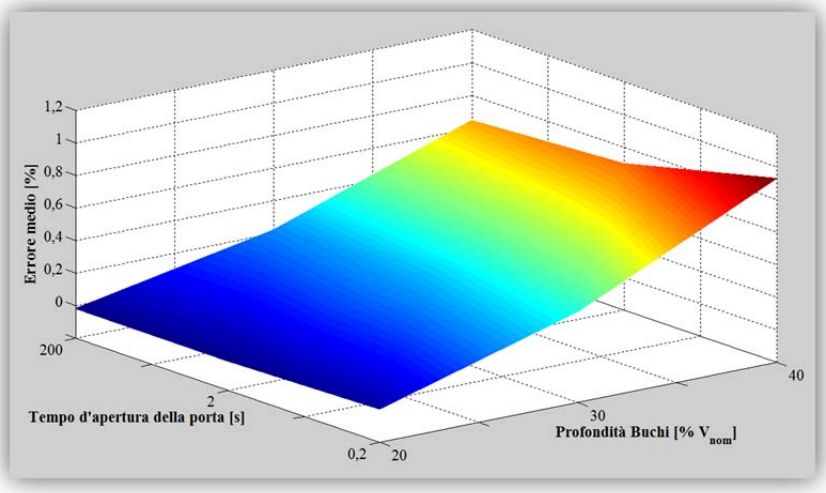

Fig. I-15: Mean error vs. voltage dip depth and gate time; Dip duration: 1s

II. Power quality measurement methods

Electrical measurement on power systems, in non-sinusoidal conditions, requires suitable instrumentation supported by theoretically correct methods. To solve this problem some standards are published by the international committees, such as the standard CEI EN 50160 and IEC 61000-4-30.

1. Standards

- ✓ The standard CEI EN 50160 defines the main characteristics of the supply voltage for public MV/LV distribution users in nominal operating conditions. It reports the limits in which remain the characteristics of supply voltage in nominal operating conditions;
- ✓ The standard IEC 61000-4-30 defines the methods for measurement and interpretation of results for power quality parameters in 50/60 Hz a. c. power supply systems. Measurement methods are described for each relevant type of parameter in terms that will make it possible to obtain reliable, repeatable and comparable results regardless of the compliant instrument being used and regardless of its environmental conditions.

Really all the 61000 standard series provides methodologies for certified measures of power quality disturbances.

In the standard IEC 61000-4-30 For each parameter measured, two classes of measurement performance are defined.

- Class A performance

This class of performance is used where precise measurements are necessary, for example, for contractual applications, verifying compliance with standard CEI EN 50160, resolving disputes, etc. Any measurements of a parameter carried out with two different instruments complying with the requirements of class A, when measuring the same signals, will produce matching results within the specified uncertainty. To ensure that matching results are produced, class A performance instrument requires a bandwidth characteristic and a sampling rate sufficient for the specified uncertainty of each parameter. As regard the

measurement of the magnitude of the supply voltage it needs to measure the *rms* value and the measurement uncertainty ΔU shall not exceed $\pm 0,1\% V_{nom}$; Whereas the basic measurement of a voltage dip and swell shall be the $U_{rms(1/2)}$ on each measurement channel and the measurement uncertainty ΔU shall not exceed $\pm 0,2\% V_{nom}$.

- Class B performance

This class of performance may be used for statistical surveys, trouble-shooting applications, and other applications where low uncertainty is not required. As regard the measurement of the magnitude of the supply voltage it needs to measure the *rms* value and the measurement uncertainty ΔU shall not exceed $\pm 0,5\% V_{nom}$; Whereas the basic measurement of a voltage dip and swell shall be $U_{RMS(1/2)}$ on each measurement channel and the measurement uncertainty ΔU shall not exceed $\pm 1\% V_{nom}$.

Also the standard gives constraints on the measurement time interval for parameter magnitudes (supply voltage, harmonics, interharmonics and unbalance). For class A performance they shall be a 10-cycle for 50 Hz power system or 12-cycle for 60 Hz power system. In addition measurement time intervals are aggregated over 3 different time intervals that are:

- 3-s interval (150 cycles for 50 Hz nominal or 180 cycles for 60 Hz nominal);
- 10-min interval,
- 2-h interval.

For class B performance the manufacturer shall indicate the method, number and duration of aggregation time intervals.

2. Certification

The requirement of certificated measurement has led to create test laboratories that can provide measures in class A as required by the standards. As regard, during my Ph.D course, I partecipated to the accreditation process, according to

the ‘ISO/IEC 17025’ standard, of the ‘*PowerLab*’(Fig. II-1) that is an university test laboratory that provides certified power quality measurement.

Fig. II-1: logo of the PowerLab

3. Instrumentation for power quality disturbances measurements

The instrument used by the laboratory that is the main instrument for this kind of measures is the so-called ‘*network analyzer*’. Its functionality can be divided into:

- data logging,
- Inspection in local,
- Both functions

In Fig. II-2 the typical block diagram of a network analyzer is shown.

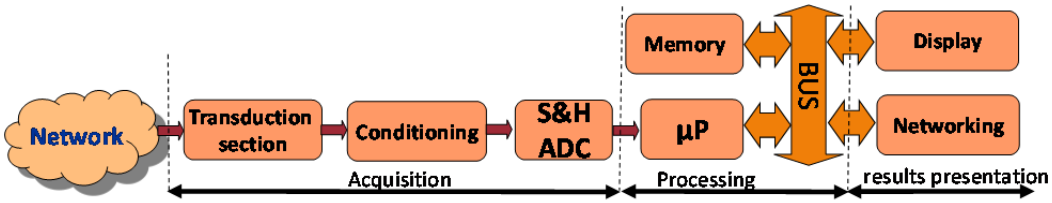

Fig. II-2: Typical block diagram of a network analyzer

A problem of such measures is related to the time used for manage a commission. In particular the time interval from when the instrument is positioned and configured until it is withdrawn by the customer. Analyzing the time intervals imposed by the standard CEI EN 50160 for voltage dips and swells measurement, these are very long, up to one year. So Using performing but expensive

instruments, a test laboratory is not able to be competitive in the market or it is not able to handle multiple commissions at the same time.

So in this PhD cycle I worked on the aspects of the implementation of a low-cost, microcontroller-based, distributed network analyzer. Its main characteristics are:

- to make simultaneous acquisition, thus no phase errors between voltage and current signals are performed;
- to process data simultaneously with the acquisition in order to keep real-time constraints;
- Publication of data via the web both to overcome the memory limitations of this type of hardware and to perform the periodic check about the state of the system and the statistics of measurement

4. Low-cost network analyzer

A. Details

The network analyzer is able to measure the power quality characteristics by each appliance during time periods. Furthermore, it is possible send data via Ethernet to a web server. The network analyzer proposed measures, in a given period of time, the following parameters:

- Frequency;
- Power Quality;
- Voltage and Current root mean square (RMS) values (V_{RMS} and I_{RMS});
- Active Powers (P) and Power Factor (PF);
- Voltage and Current Total Harmonic Distortions (THD_V and THD_I);
- Energy consumption;
- Power consumption profile.

The user is able to see the daily consumption and the power system state by means of displays installed at near the measurement points. In this way it is possible the inspection in local. Furthermore in this thesis is proposed a web portal where customers are able to perform the periodic check about the state of the system and the statistics of measurement.

B. Hardware Architecture

In “Fig. II-3”, the architecture of the distributed system is shown. The analyzers can communicate between them. The communication is bidirectional: in this way, it is possible to exchange information between the various meters.

The “Fig. II-4” shows the schematic of the developed system. Each meter has an information display. Every group of meters includes a data aggregator, which communicates with components in the group. Information display, meters and data aggregator communicate with each other through the power line. Additionally PLC repeater can be installed if the distance between meters and data concentrator is excessive or there is a physical problem making the communication difficult, (not necessary for normal apartment building). These equipment can be installed anywhere and in several types of configurations as shown in “Fig. II-4”. Also a Web Server (installed in data aggregator) can provide internet communication to provide measurement statistics for a single meter or for a group of meters. STM32F103xxx is used as core of the hardware platform [5], [6].

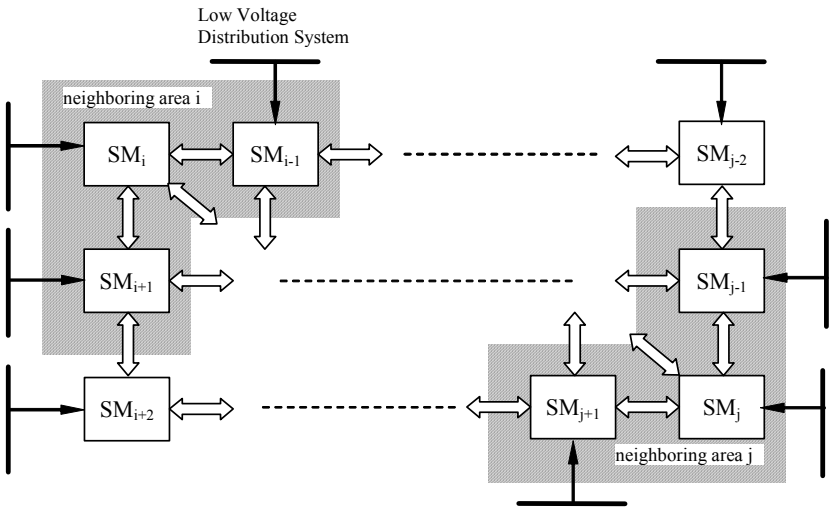

Fig. II-3: Architecture of the proposed distributed network analyzer

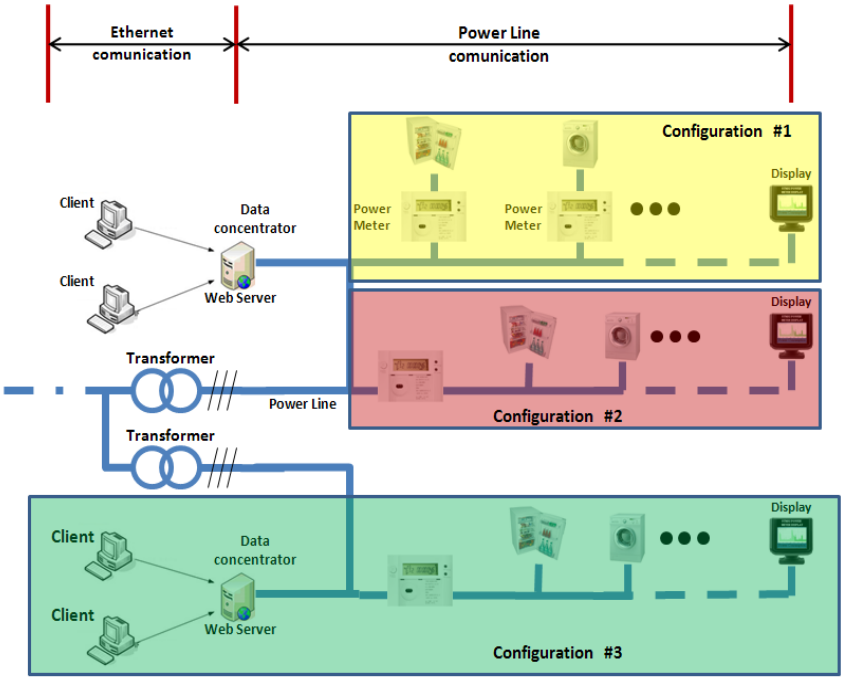

Fig. II-4: Configuration types of the system with communication components

The STM32 is based on the Cortex-M3 profile, which is specifically designed for high system performance combined with low power consumption.

The heart of the STM32 is the Cortex-M3 processor. The architecture of the microcontroller is shown in "Fig. II-5". The Cortex M3 processor is a standardized microcontroller including 32 bit CPU, bus structure, nested interrupt unit, debug system and standard memory layout. The Cortex processor benchmarks give a performance level of 1.25 DMIPS/MHz, which is 1.2 Clock cycles per instruction. The STM32 operates up to CPU clock speeds of 72MHz, it offers FLASH ROM sizes up to 512K (Program) and 64K SRAM (Data), Dual 12bit ADC with input range of 0÷3.3 V, general purpose timers, I2C, SPI, CAN, USB real-time clock and Ethernet Interface. The STM32 is composed of the Cortex core which is connected to the FLASH memory by the dedicated Instruction bus. The Cortex Data and System buses are connected to a matrix of ARM Advanced High Speed Buses (AHB). The internal SRAM is connected directly to the AHB bus matrix, as is the DMA unit. The peripherals are located on two ARM Advanced Peripheral Buses (APB). Every APB is bridged onto the

AHB bus matrix. The AHB bus matrix is clocked at the same speed as the Cortex core. However, the AHB buses have separate prescalers and may be clocked at slower speeds to preserve power. It is important to note that APB2 can run at the full 72MHz while APB1 is limited to 36MHz. Both the Cortex and the DMA unit can be bus masters. Because of the inherent parallelism of the bus matrix, they will only arbitrate if they are both attempting to access the SRAM, APB1 or APB2 at the same time. However, the bus arbiter will guarantee 2/3 access time for the DMA and 1/3 for the Cortex CPU. Microcontroller is a programmable system according to the specific application. STM32 can be programmed entirely in C++ code through development environments which allow debugging by JTAG interface. After Reset STM32 is able to work autonomously, being a stand-alone system

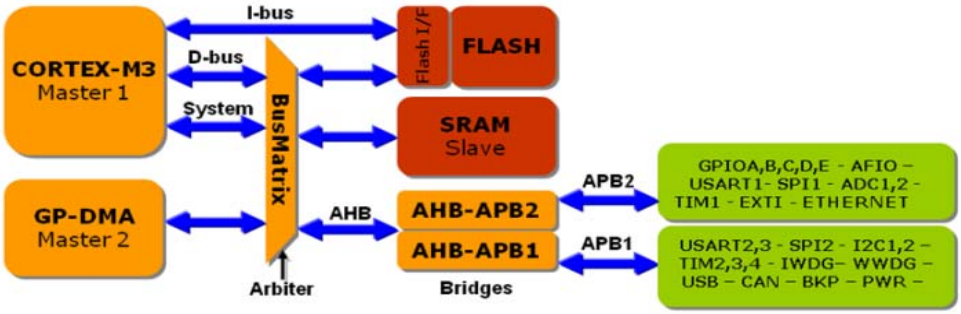

Fig. II-5: STM32 Architecture

C. Software implementation

In the "Fig. II-8", the real time software instrument implementation is shown. Referring to the standard IEC 61000-4-30 [7], the power quality parameters considered are:

supply voltage dips and swells, voltage interruptions, voltage transients, fundamental frequency, supply voltage, power factor, magnitude of the supply voltage, voltage and current harmonics and interharmonics. From Channel in, the samples are acquired with a sampling frequency of 1MS/s. This samples are processed with a low-pass filter with 10 kHz cut-off frequency (Section A-B), averaged and decimated in order to increase the resolution for the following analyses which require 9kHz frequency band at least. Then, the samples are

buffered (Section C). In signals acquiring we used two ADCs with two S&H. We programmed ADCs to make simultaneous acquisition, thus no phase errors between voltage and current signals are performed.(Fig. II-6)

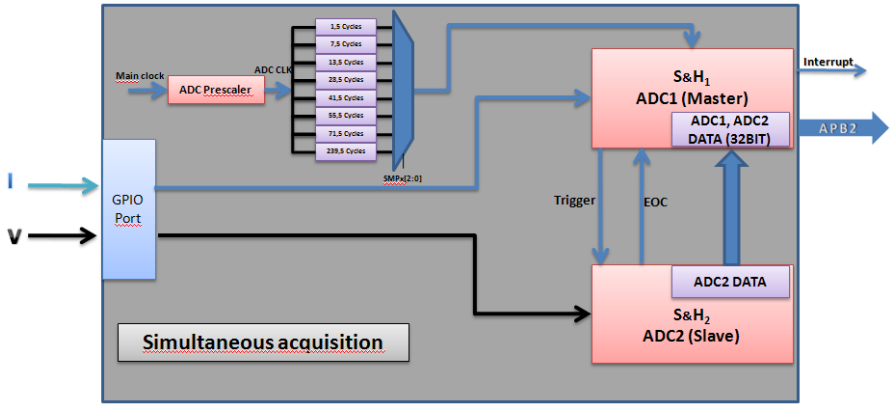

Fig. II-6: Acquisition

After each conversion cycle, ADC1 (Master) send an interrupt to DMA device, which will transfer both ADC1 and ADC2 samples from "ADC1 Data Register" to a memory buffer. DMA fills a buffer in circular mode (at the end of buffer, transfer continues starting all over again). Moreover DMA send two interrupts to CPU called "Half_Buffer" and "Buffer_Full", so in its service routine, CPU treats data of that part of buffer. In each service routine CPU will treat a number of samples equivalent to more than ten period of a frequency signal 50Hz. So the time between two interrupt (Half – Full or Full – Half) is $T_A > 0.2s$. In order to keep real-time constraints, CPU performance and algorithm efficiency will have to ensure an elaboration time $T_E < T_A$ (Fig. II-7).

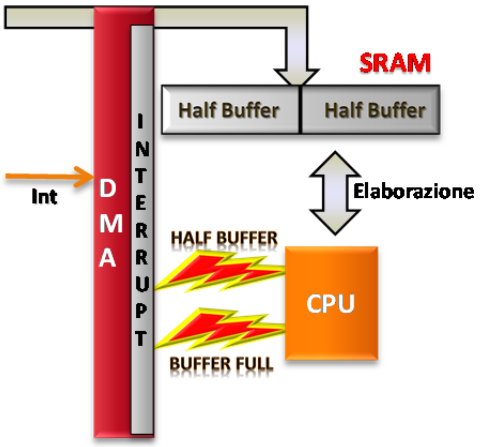

Fig. II-7: memory management

The block D is used to estimate the actual fundamental frequency in order to perform synchronized analyses. The section E looks for dips through rms continuous processing. In the block G, a digital re-sampling is made to obtain in exactly ten cycles of the fundamental a number of samples that is a power of two. The result of all the measurement sections are validated using flag control: flagged results are not accounted for subsequent analysis, not flagged data are grouped with reference to absolute time in order to obtain measurement with 10 min clock boundary [8].

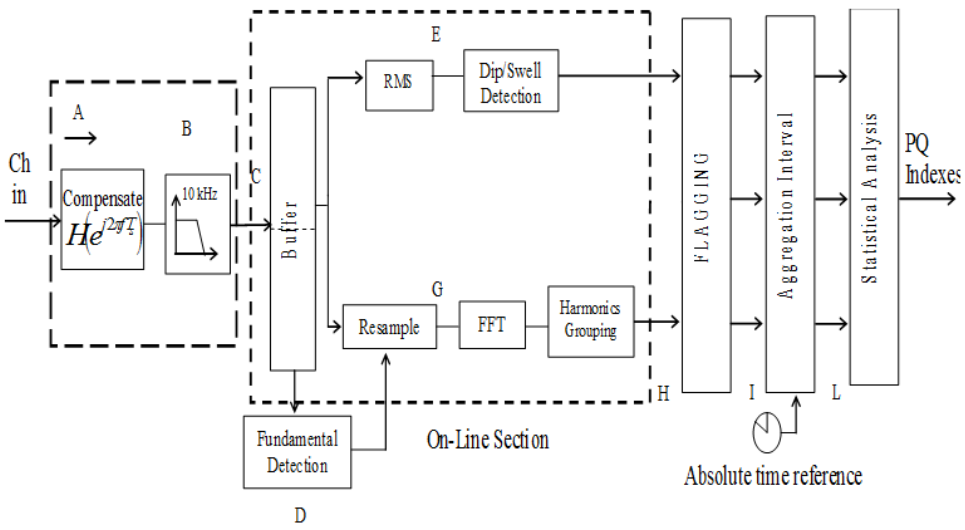

Fig. II-8: Software architecture

D. Metrics

Metrics implemented in the firmware are:

RMS values of voltage and current:

$$V_{rms} \simeq \sqrt{\frac{1}{N}\sum_{k=0}^{N-1} V_k^2}\,; \qquad I_{rms} \simeq \sqrt{\frac{1}{N}\sum_{k=0}^{N-1} I_k^2} \tag{1}$$

Active power:

$$P_a = \frac{1}{T}\int_0^T v(t)\cdot i(t) \simeq \frac{1}{N}\sum_{k=0}^{N-1} V_k \cdot I_k \tag{2}$$

Apparent power:

$$P = V_{rms} \cdot I_{rms} \tag{3}$$

Total harmonic distortion for voltage and current:

$$THD_V = \sum_{h=2}^{M} \frac{V_{h,rms}}{V_{1,rms}} \tag{4}$$

$$THD_I = \sum_{h=2}^{M} \frac{I_{h,rms}}{I_{1,rms}} \tag{5}$$

5. Communication network

Distributed meters transfer measurement results to the data aggregator via CAN protocol. In the data aggregator a web server collects the statistics of each meter and other advanced information is extracted. A client can connect to the server to analyze meter group measurement results.

A. Local area Communication interface

The implemented distributed network analyzer requires a reliable communication low level interface. Its main required features are: i) low cost implementation ii) noise immunity iii) easy configuration iv) multicast network. For these reasons we chose the CAN protocol. It was specifically designed to operate seamlessly even if highly disturbed by the presence of electromagnetic disturbances thanks to the adoption as a means of transmission a line with potential difference balanced

signals. The immunity to electromagnetic interference can be further increased by using twisted pair cables. The bit rate can be up to 1 Mbit/s to less than 40-meter nets. Slower speeds let you reach greater distances (125 kbit/s to 500 m) as in the considered case.

The simplified architecture of implemented CAN interface is shown in the Fig. II-9. The communication protocol implements a priority based bus arbitration mechanism. It means that a message with numerically smaller values of ID have higher priority and are transmitted first.

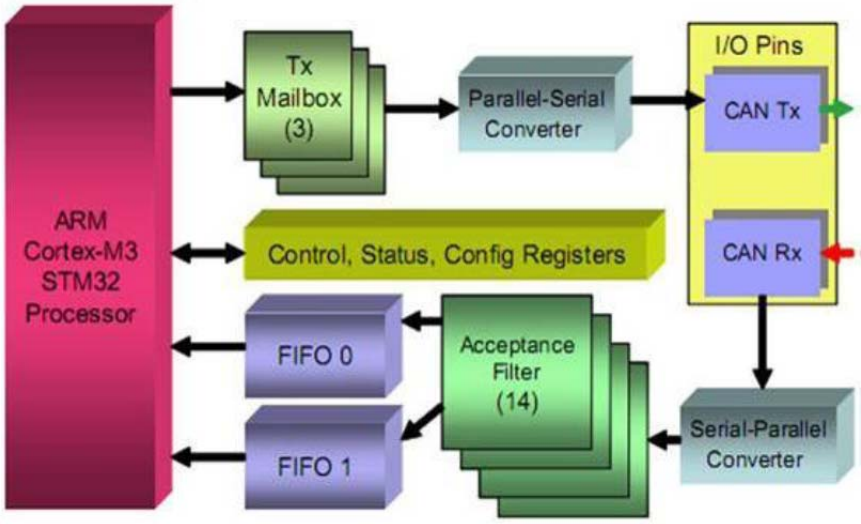

Fig. II-9 the implemented CAN architecture

In more detail, if the bus is idle, any node may begin to transmit. If two or more nodes begin sending messages at the same time, the message with the higher id (which has more dominant bits, i.e., zeroes) will overwrite other nodes lower id's, so that eventually (after this arbitration on the id) only the dominant message remains and is received by all nodes.

The communication handshake in described in the following. The master microcontroller sends a message, with a “remote frame”. It is a message without information content, aimed to request a Data Frame from the slaves.

Three transmit mailboxes are provided to the software for setting up messages. The transmission Scheduler decides which mailbox has to be transmitted first, for

example the Energy consumption of a single load. The message is converted by a parallel-serial converter and it is sent to the CAN TX Pin.

The master microcontroller receives the Remote Frame through the Pin CAN Rx. After, the message is converted in parallel through a serial-parallel converter. The frame is sent to an Acceptance Filter that is composed of 14 configurable identifier filter banks for selecting the incoming messages the software needs and discarding the others. Two receive FIFOs are used by hardware to store the incoming messages [12]. Three complete messages can be stored in each FIFO. The FIFOs are managed completely by hardware.

When a Remote Frame is received, the microcontroller sets up a response message, a Data Frame corresponding to the Remote Frame, and sends it to the microcontroller that previously sent the Remote Frame. The structure of the Data and Remote frame is the following:

The Start of Frame denotes the start of the Frame transmission. The ID is the identifier for the data and also represents the message priority. The Remote Transmission Request is set to dominant (zero). The Identifier extension bit and Reserved bit must be dominant (zero). The Data Length Code consists of four bits and indicates the number of bytes of data (0-8 bytes). The Data Field denotes the data to be transmitted (0-8 bytes) and it only is in the Data Frame. The Cyclic Redundancy Check, composed by 15 bits, is an error–detecting code using to detect accidental changes to raw data. The ACK slot is sent recessive (1) from the transmitter and any receiver can assert a dominant (0) and the End of Frame must be recessive (1).

Distributed energy meters transfer measurement results to the data aggregator through CAN protocol. In the Fig. II-10 is reported as an example with two slave microcontrollers that continuously acquires voltage and current signals and calculate their RMS values, the Power Factor and the Active Power (P), showing them on the display. When the master sends a Remote Frame to the slave to know measured Active Power, the slave microcontroller sends in the Data Field the value of the Active Power. The master receives the data and sends them to the display. The estimation of transmission time was possible adopting the

microcontroller DAC. In particular, a single bit of the DA converter has been used to generate a square wave. The result has been calculated through the oscilloscope Tektronix TDS3012B.

Several tests have been performed to characterize the transmission time. A first test was made to calculate the delay between the instant when the master microcontroller sends the request and the instant when a slave detects an interrupt for the reception of the request. The estimated time is approximately 3.6 ms. Further tests were performed considering the data aggregator and two slave meters. The data aggregator requires data relating to the active power to both with two different priority levels. It receives data from the slave with the highest priority approximately after 25 ms those relating to the second after approximately 60ms. In fact, the waiting time for the second slave is approximately 35ms. The time latency was calculated through the microcontroller DAC. In particular, a single bit of the DAC has been used to generate a square wave. The results have been calculated through the oscilloscope Tektronix TDS3012B.

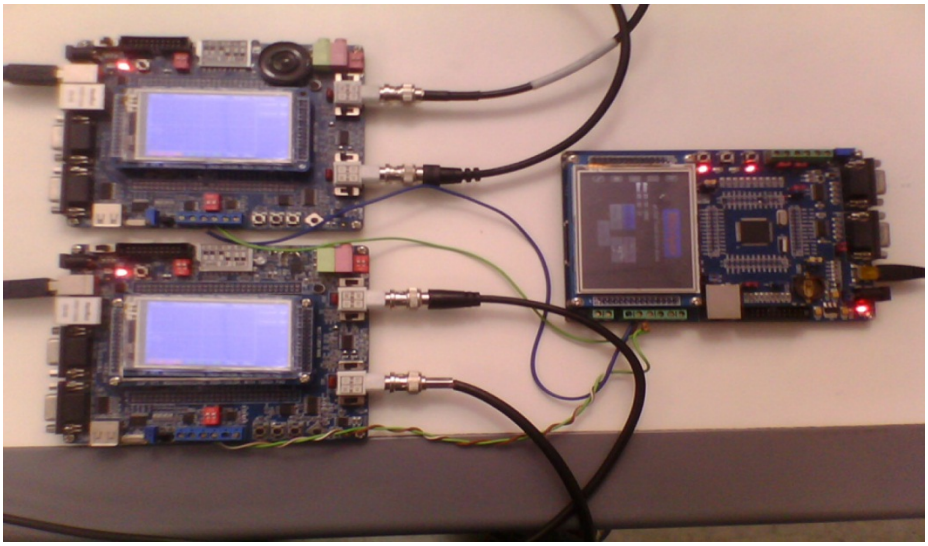

Fig. II-10: Example of data transmission

B. The implemented Web-Server

In the data aggregator a web server collects the statistics of each meter and extracts other information [13]. Through the web server, the user can monitor the power quality profile of a single load [14].

HTTP web server has been implemented. It can serve dynamic web pages and files from a read-only ROM file system, and provides several scripting languages.

For the power consumption request the steps of the CGI are the following:

i) User click Power Graph;

ii) Client Browser;

iii) Sent Request at the Web Server.

After the Web Server:

i) Loads the Routine Management UIP Packet;

ii) Check UIP Packet;

iii) Starts the Routine Httpd_add_call;

iv) Checks the request (Power Graph)

The Service Procedure of the Script is the sequent:

i) Sends the file header.html;

ii) Writes the text “Power Profile Load”;

iii) Calls the function Create Graph;

iv) Terminates the script.

In the development of Web Server application HTML protocol is used to provide static web pages to the client. In “Fig. II-11” the web server work process is shown [9].

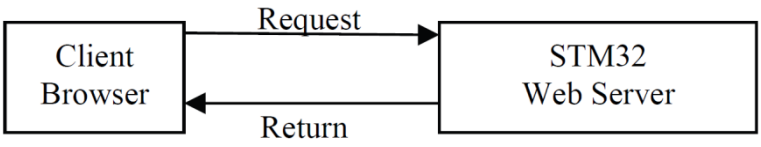

Fig. II-11: Work process

Concrete steps are:

i) user, in the client browser, makes a request to the Web Server;

ii) Web Server will make a judgment on the request;

iii) Web Server will transfer the files directly to the client browser.

Each web page consist of two parts:

i) The header part contains the title of the website and several links to view other pages;

ii) The latter part contains the linked pages.

In Fig. II-12 the home page is shown.

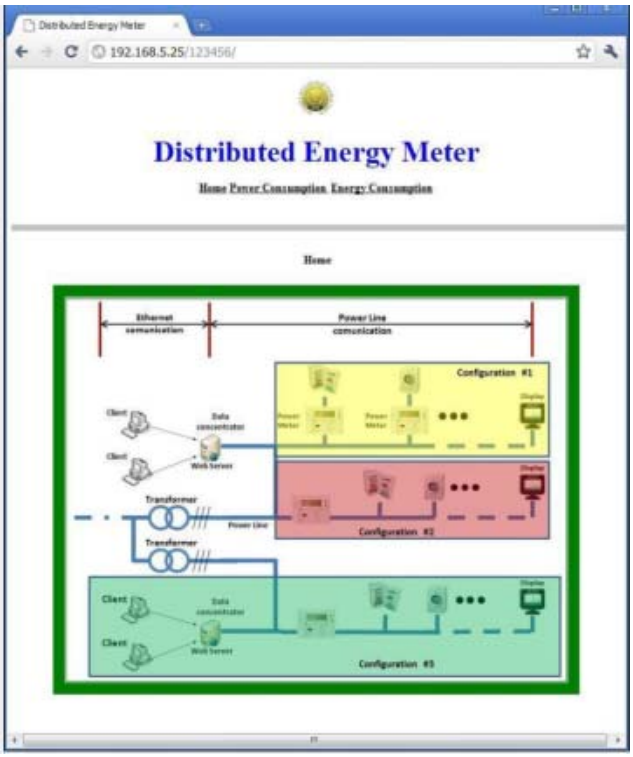

Fig. II-12: The Home Page

6. Experimental result

In order to prove reliability of the implemented instrument a characterization has been performed. Tests have been executed generating two sinusoidal signals, varying amplitudes, frequency and relative phase angle. These preliminary tests have been carried out without sensing and conditioning sections, using as reference values the measurement results of a PXI platform with high performance data acquisition system. The automatic test equipment is shown in Fig. II-13.

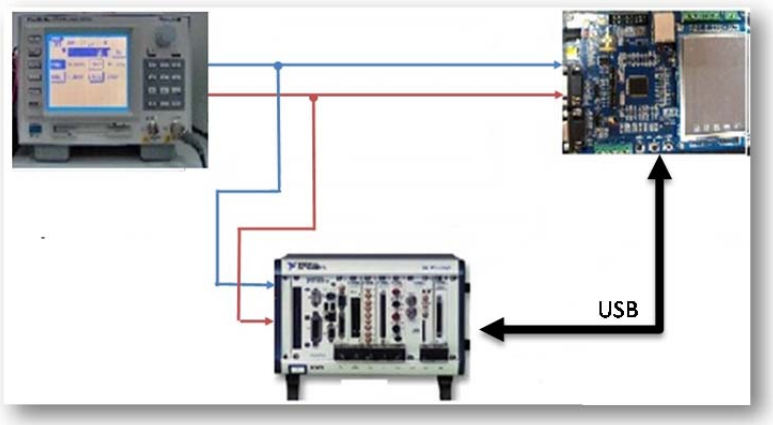

Fig. II-13: Instruments for experimental tests

The first test has been aimed to verify performance of AD converters. Eleven dc values have been generated in the input range of the ADCs, i.e. 0÷3.3 V, and the mean relative deviations with respect to full scale (F.S.) range have been measured. The results are shown in Fig. II-14: deviations are included in the range -0.1÷0.7 %.

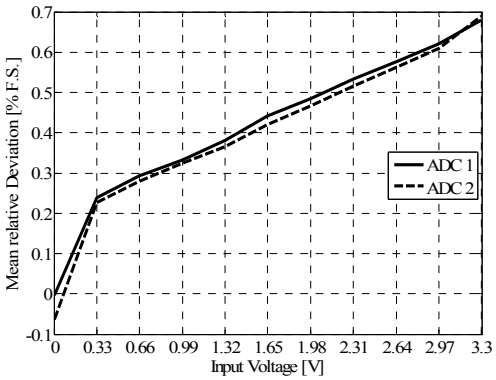

Fig. II-14: Static characteristics of the two ADCs of the microcontroller

Linear characteristics in almost all of voltage range is shown. Only around about zero, ADCs transfer characteristics is not linear. However, in respect of IEC 61000-4-30, the peak voltage must be equal to half of full scale: voltage range in which ADCs have to work is $\Delta V = 1.65 \pm 1.65/2 = 0.825 \div 2.475\ V$. In order to compensate ADCs gains and offsets, ADCs transfer characteristics have been fitted with linear functions considering only input range of the ADCs 0.33÷3.3 V.

The results are shown in Fig. II-15: deviations are included in the range -0.01÷0.01 %.The corrected sample values are therefore used to calculate all the measurement quantities.

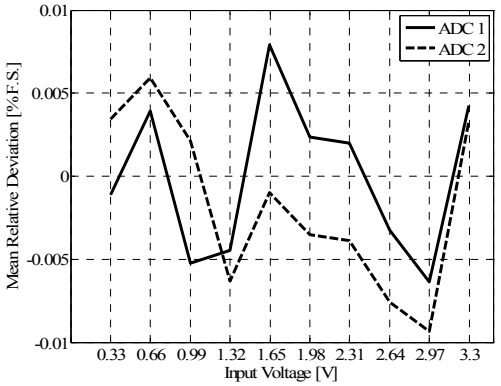

Fig. II-15: Static characteristics of the two ADCs of the microcontroller after Fitting

In the second test, RMS voltage and current, active power, apparent power and frequency measurements have been verified. Sinusoidal waveforms, with frequency in the range of 42.5÷57.5 Hz and peak-to-peak amplitudes to 1.65 V, have been generated. The results of frequency deviation are shown in Fig. II-16 . in the same figure the range of standard deviation is also shown: it is included in the range of ±0.07 %.

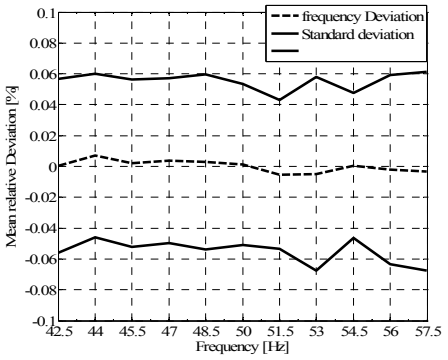

Fig. II-16: Mean relative deviations on frequency measurement

The results of RMS voltage and current, power active and apparent power measurements, with relative standard deviations are shown in Fig. II-17, Fig.

II-18, Fig. II-19, Fig. II-20: they have been calculated as percentage of instrument full scale; their mean relative deviation are in range ±0.01 % F.S.

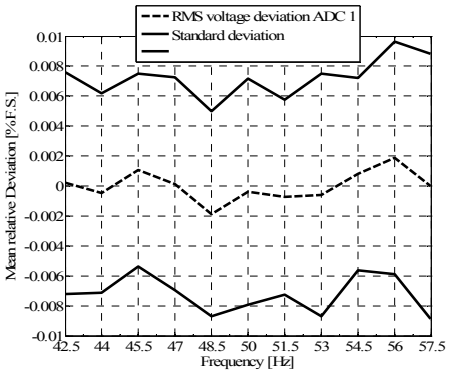

Fig. II-17: Mean relative deviations on RMS Voltage measurement

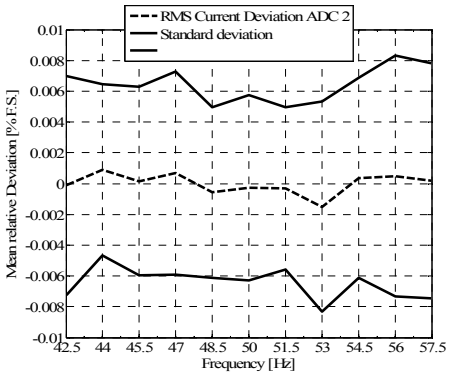

Fig. II-18 Mean relative deviations on RMS Current measurement

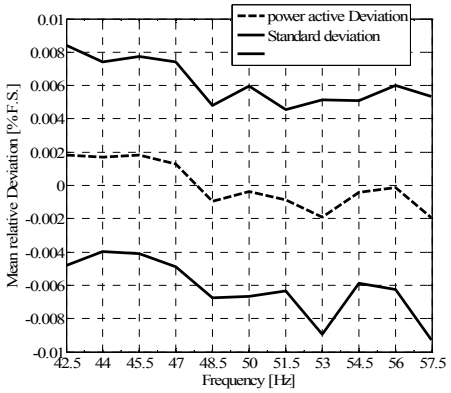

Fig. II-19 Mean relative deviations on active power measurement

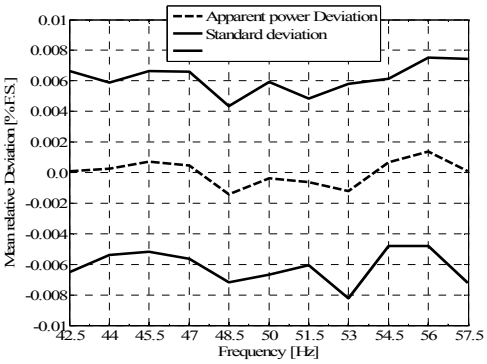

Fig. II-20 Mean relative deviations on apparent power measurement

In the third test, THD measurement has been verified. deformed waveforms, composed by two Harmonics: fundamental harmonic with frequency of 50 Hz, non-fundamental harmonic with frequency in the range 100÷1250 Hz; and peak-to-peak amplitudes to 1.65 V, have been generated. The results of voltage and current THD with relative standard deviations are shown in Fig. II-21 and Fig. II-22: deviations do not exceed are included the range of ±0.2 %.

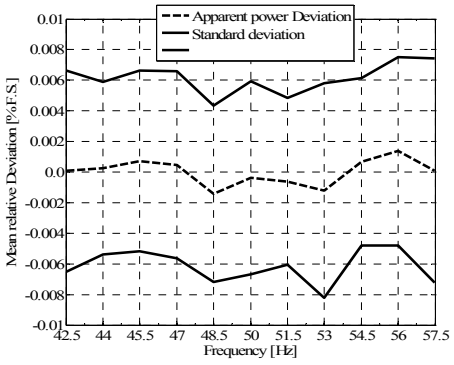

Fig. II-21: Mean deviations on THD Voltage measurement

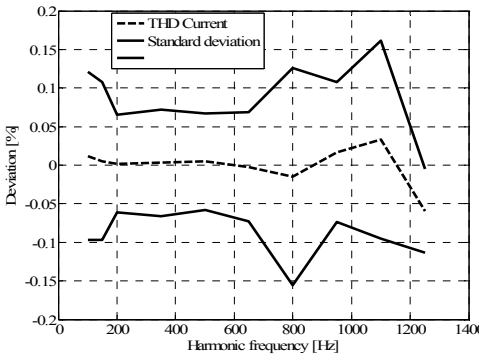

Fig. II-22: Mean deviations on THD Current measurement

In the fourth test, THD voltage and current, RMS voltage and current, active power, apparent power and frequency measurements in distorted regime have been verified. Distorted waveforms, composed by a fundamental harmonic component with frequency in the range of 42.5÷57.5 Hz and peak amplitude to 0.825 V, and third harmonic component with frequency to 150 Hz and peak amplitude to 10% of fundamental harmonic (0.0825 V) have been generated. The results of frequency deviation are shown in Fig. II-23 . in the same figure the standard deviation, included in the range of ±0.3 %, is also shown. The results of RMS voltage and current, power active and apparent power measurements are shown in Fig. II-24, Fig. II-25, Fig. II-26: they have been calculated as percentage of instrument full scale.

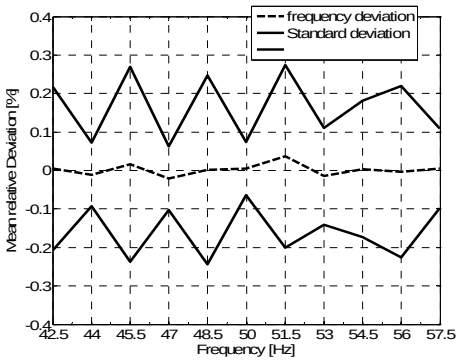

Fig. II-23Mean relative deviations on frequency measurement

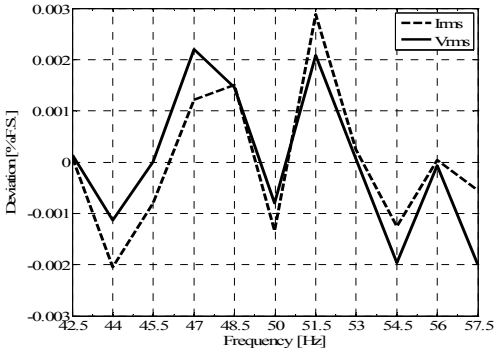

Fig. II-24 Mean relative deviations on RMS Voltage and Current measurement

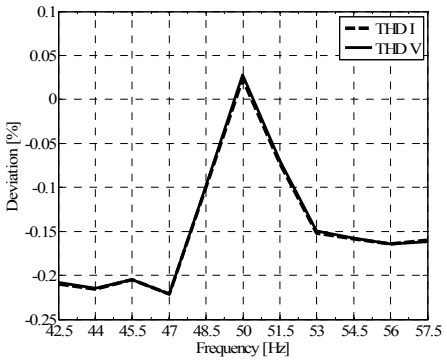

Fig. II-25 Mean deviations on THD Voltage and Current measurement

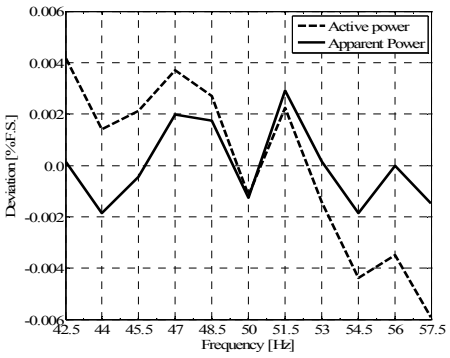

Fig. II-26. Mean relative deviations on active and apparent power measurement

Then, a simple web server has been implemented. The home page is shown in the Fig. II-12. The webpage address is composed by an ip address (192.168.5.25 in the example) followed by a password (123456 in the example). In this simple example, the webpage is divided in two parts: the header part contains the title of the website and several links to view other pages: this part is the same in all the web pages; the latter contains the linked webpage. In addition a typical daily power consumption in a generic meter is shown in Fig. II-27. The peak value of the consumption is in the central hours of the day as shown in the figure.

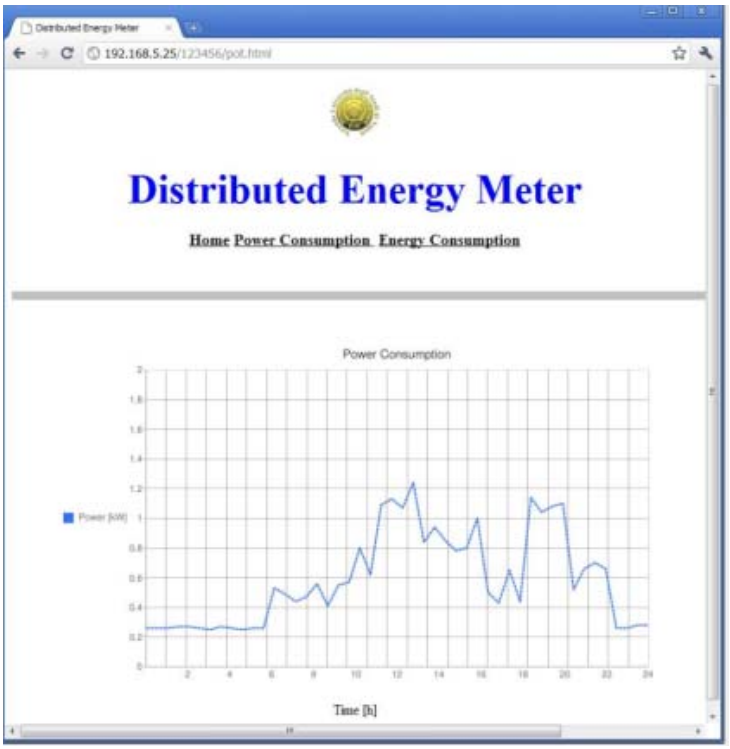

Fig. II-27: Daily power consumption in a generic house

III. An efficient pre-processing scheme to enhance resolution in band-pass signals acquisition

1. Introduction

As the great majority of electronic instrumentation is nowadays digital, data acquisition plays a key role in their performance. Data acquisition systems (DAS's) are, in fact, the core of complex instruments, such as digital oscilloscopes and data/protocol analyzers, as well as an essential part cascaded to the superetherodyne receiver in the hybrid architecture of performance spectrum analyzers and vector signal analyzers. The accuracy of all the aforementioned instruments is limited by the internal DAS performance.

Since the advent of DAS's, their architectures have included an analog-to-digital converter (ADC) and an embedded microcontroller for control operations. The most recent integrated circuit (IC) technology progresses have largely expanded DAS's potentialities with respect to their earliest implementations. At present, IC technology permits to assemble several interleaved ADCs that realize a unique fast ADC, with sample rate up to 100 GS/s at a nominal resolution of 8 bits.

Modern DAS's can suitably condition the flow of measurement data by using microprocessors, which have relevant digital signal processing capabilities, in place of microcontrollers. At the same time, the gap between the limited data routing speed of microprocessors and the superior one of fast ADCs in data storage is partially compensated by means of a sophisticated computer built around microprocessors [15].

In the past, control and processing operations used to take more time than the acquisition itself, when running at the highest sample rate. The maximum data capture rate, i.e. the maximum number of record acquisitions per unit of time, was thus strongly limited. Nowadays, the powerful processing capabilities of the embedded computer make higher capture rates possible. Further improvements that are enabled by the most recent DAS's architecture, which is sketched in Fig. III-1, also include: (i) higher waveform rate; (ii) deeper memory records management; (iii) quick responsiveness; (iv) inclusion of measurement and statistics capabilities, such as Fourier analysis, which are built-in, i.e.

implemented in the firmware; (v) transfer of data records to an auxiliary host, through high-speed data buses, which can be useful for complex processing of the acquired signals.

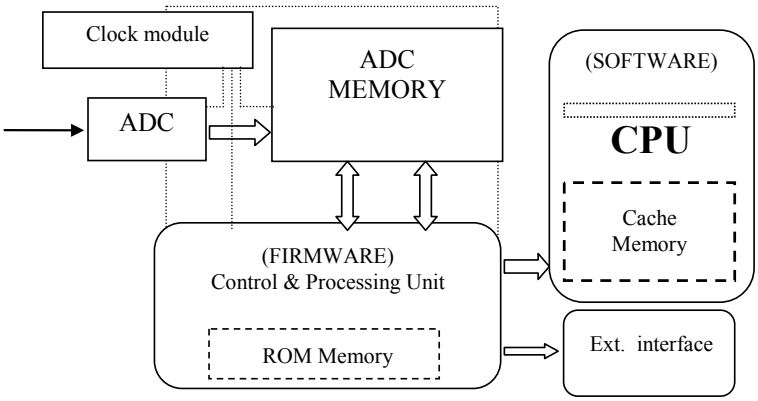

Fig. III-1: Modern DAS architecture.

The available data processing capabilities can also be exploited for improving the performance of DAS's in terms of vertical resolution. Such idea has partially been implemented by some major manufacturers, who placed on the market digital storage oscilloscopes with built-in *high resolution* or *enhanced resolution* acquisition modes, in the late '90s [16], [17]. These acquisition modes take advantage of oversampling and low-pass filtering operations to achieve improved effective number of bits (ENOB) and signal-to-noise-and-distortion-ratios (SINAD) in data acquisition. Such solutions are implemented through a few very simple operations so as not to determine a heavy additional computational burden on the acquisition system. Moreover, *high resolution* or *enhanced resolution* acquisition modes can improve ENOB and SINAD only in the analysis of base-band signals. Details on the definitions of ENOB and SINAD and the related testing techniques are given in the next Section. No built-in solution, optimized for the analysis of band-pass signals, has been presented yet. Indeed, band-pass signals with high bandwidth-to-carrier frequency ratio are very common in nowadays communication systems and measurement solutions for such signals would benefit from a resolution enhancement [18-26]. In this regard, exploiting

band-pass sampling is not an optimal choice, as it causes a degradation of the signal-to-noise ratio [27-33].

On the contrary, it can be shown that nowadays technology is adequate to extend the concepts of *high resolution* or *enhanced resolution* to band-pass signals. Designing a data acquisition system that selects the most proper setup for improving the vertical resolution, according to the bandwidth of the input waveform can now effectively be pursued.

In this chapter a novel architecture for a DAS with built-in resolution enhancement functionalities optimized for band-pass signals is presented. The basic novelty of the proposed approach is to extend the idea of oversampling and subsequent filtering which is behind the enhanced resolution techniques available on top-level general purpose DAS's to the case of band-pass signals. It will be shown that the more *band-pass* is the signal, the higher is the improvement achievable in the resolution. The solution extends the theory presented in [34]. In particular, the proposed solution is founded on a similar basic architecture, but comes out to be more user-friendly, as it only requires the user to indicate the signal's spectral occupancy and then automatically sets the filter parameters. An analytical comparison of the resolution improvement achievable by means of the proposed solution with respect to existing resolution improvement techniques is also shown, as a function of the signal's parameters. Moreover, a number of experiments are discussed to assess the performance of the proposed solution.

The chapter is organized as follows. Section 2 gives some notes on performance metrics and provides a theoretical estimation of the achievable resolution improvement as a function of the bandwidth of the acquired signal. Section 3 introduces the proposed architectural solution and evaluates the resolution improvement achievable. Section 4 gives the results of the performance assessment, based on both simulation and instrumental experiments.

2. DAS performance: metrics and resolution improvement

The performance of DAS's mostly depends on that peculiar of the inner ADC along with the associated processor. Many parameters and testing techniques defined to evaluate ADC performance can be referred to DAS's [28], [34-37]. It has to be noted, however, that the theoretical limits initially established for ADC parameters, can be overtaken by the data processing capabilities allowed by the DAS, depending on the characteristics of the signal that is acquired.

In the following subsection, few notes are given on two key ADC performance metrics, i.e. ENOB and SINAD, which are defined in IEEE Standard 1241-2000 [37] as:

- **effective number of bits (ENOB)**: A measure of the signal-to-noise and distortion ratio used to compare actual analog-to-digital converter (ADC) performance to an ideal ADC;
- **signal-to-noise and distortion ratio (SINAD)**: For a pure sine wave input of specified amplitude and frequency, the ratio of the root-mean-square (rms) amplitude of the analog-to-digital converter output signal to the rms amplitude of the output noise, where noise is defined as above to include not only random errors but also nonlinear distortion and the effects of sampling time errors. (Note that signal-to-noise and distortion ratio in IEEE Std 1241-2000 is equivalent to signal-to-noise-ratio in IEEE Std 1057-1994).

ENOB and SINAD quantify the effects of dynamic errors occurring when high-frequency signals are acquired. The improvement granted by the proposed solution will be quantified in the experiments in terms of improvement of such metrics.

The second subsection explains the way at present data processing makes DAS's available on the market capable of offering higher resolution than their underlying ADC's.

A. Testing techniques for ENOB evaluation

Along with quantization noise, there are several non-idealities that have effect on the performance of an ADC, such as INL, DNL, missing codes, aperture jitter, etc.

[37],[38]. Evaluating the ENOB is a direct way to globally quantify the dynamic performance of an ADC.

ENOB represents the resolution of an ideal converter whose quantization noise is equal to the total noise of the converter under test. In other words, saying that the ENOB of an ADC is equal to *k* means that the converter performs as an ideally perfect converter with a resolution of *k*. ENOB is defined as:

$$ENOB = n - \log_2\left(\frac{N}{Q}\right) \tag{1}$$

where *n* represents the nominal number of bits of the ADC, *N* is the *rms* value of the total noise, and *Q* is the *rms* value of the quantization noise of an ideal *n*-bit ADC when a full-scale sinusoidal signal is acquired.

ENOB is measured according to a standard procedure: a full-scale sine-wave is given in input to the converter; the waveform is acquired, and the best fitting sine-wave is found out by means of a curve fitting algorithm; the evaluation of the total noise N is obtained by subtraction.

As well known, the rms value Q of the quantization noise of an ideal converter is estimated as

$$Q = \frac{\Delta}{2\sqrt{3}} \tag{2}$$

that is the standard deviation of a random stationary process with a uniform probability density function within the interval (-*Δ*/2, +*Δ*/2), *Δ* being the uniform quantization interval. As well known, this is the stochastic model that is usually adopted to describe quantization noise independently of the input signal.

An equivalent measure of the performance of an ADC is the signal to noise and distortion ratio (SINAD) expressed in dB, which is given by the ratio between the *rms* value of a full-scale sine-wave, *S*, and the *rms* value of the total noise, *N*, that also includes non-linear distortion and the effects of sampling time errors, *D*:

$$SINAD = 20\log_{10}\frac{S}{N+D} \tag{3}$$

SINAD and ENOB are related one to another by the equality

$$SINAD = 6.02\ ENOB\ +\ 1.76 \tag{4}$$

The constant value 1.76 dB in (4) is obtained through some straightforward calculus, and depends on the noise probability density function and is related to a full-scale usage of the converter [38]. In many applications, however, the input waveform spans just a portion of the full-scale ADC interval. This happens, for example, in the presence of signals characterized by high crest factor, or when the goal is to analyze transients superimposed to the waveform under test. The full-scale ADC is typically set at least 4 times the *rms* value of the input waveform. The additive constant in (4) is equal to 7.27 dB, in this case, i.e. the ENOB is decremented by about one unity.

B. Resolution improvement through oversampling and low-pass filtering

A common approach was introduced few years ago by some major manufacturers to improve the resolution of high performance DAS's. Basically, the idea consists in acquiring a baseband signal at a sampling frequency which is much higher than the signal Nyquist frequency f_N. Usually this sampling frequency is $f_{s,max}$, the maximum sampling frequency allowed by the DAS. Then, several consecutive samples are averaged, or more generally, a low-pass filtering is performed.

This acquisition mode is implemented in the firmware of some digital storage oscilloscope (*Hi-Res* offered by Tektronix™) and can be enabled without any restriction on the record length. A similar functionality is implemented in other widespread digital storage oscilloscopes where a weighted average is performed on a larger set of samples, which contains all the samples within the central acquisition interval and a certain number of samples that belong to the adjacent intervals. In this case, the functionality can be enabled only on data records with very limited length (*ERES* offered by LeCroy™). As an example, Fig. III-2 shows the amplitude responses of two filters: a moving average filter with length equal to 8 (trace A), and a weighted average filter, namely a hamming window, with length equal to 16 (trace B). The latter is the one characterized by superior attenuation in the stop band. The figure also shows the amplitude spectra of a sine wave acquired at two different sample frequencies, f_{S1} and $f_{S2} = f_{S1}/8$, respectively trace C and trace D. The noise level is higher for a lower sample frequency.

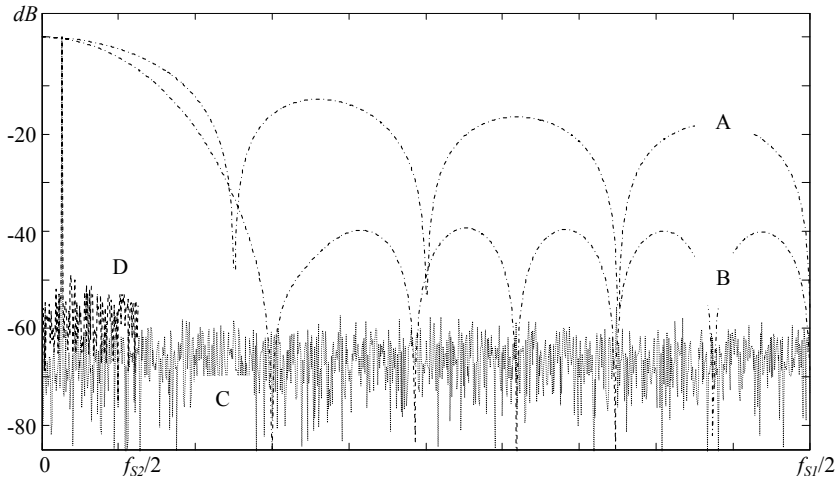

Fig. III-2: Amplitude spectra of a sine-wave acquired at two different sample frequencies, f_{S1} (C) and (D) $f_{S2} = f_{S1}/8$, and frequency response of two different low-pass FIR filters: a moving average filter with length equal to 8 (A), and a hamming window with length equal to 16 (B).

Note that the user simply has to enable or disable the aforementioned acquisition mode. According to the selected *time*/*div* setting, one or more bits of resolution enhancement are automatically obtained by the DAS, thanks to the integrated processing capabilities. The simplicity of use and the rapidity are the two main factors of strength of such solutions for resolution improvement that are currently made available on high performance general-purpose DAS's.

In order to understand how enhanced resolution is attained for baseband signals, it is convenient to consider Fig. III-2, which shows the amplitude spectrum of a full-scale sine-wave acquired by a real ADC, at two different sample rates. The figure shows a uniform noise floor. The *rms* value of the total noise, *N*, includes all the spectral contributions except for the spectral line representing the test sine-wave. The noise floor spans the whole frequency interval ranging from 0 Hz up to half the sample rate, $f_s/2$. Fig. III-2 also shows two other traces, which represent the response of two different low-pass filters, both selecting the sine-wave and a portion of the total noise. This is a typical scenario: the available sample rate of the oscilloscope is much higher than that needed to analyze the input signal. Hence, the use of digital filters in conjunction with oversampling allows resolution enhancement. In fact, oversampling smears the total noise in a larger frequency band, thus lowering its constant power density level; then, filtering

rejects the out-of-band noise and other spectral contents due to further imperfections, thus enhancing *SINAD*.

The actual *SINAD* increment depends on both the power spectral density of the total noise of the converter, and the type of digital filter, i.e. the shape and the length of its impulse response. A common schematic for estimating the achievable resolution enhancement assumes that the total noise is evenly distributed across the frequency spectrum and refers to a brick-wall filter response with upper cut-off frequency f_L. According to such a scheme, the theoretical resolution enhancement RE_{TH} due to bandwidth reduction is given by:

$$RE_{TH} = \frac{1}{2}\log_2\left(\frac{f_S}{2f_L}\right) \tag{5}$$

The resolution enhancement effect of the filtering is higher than expected if the total noise is biased toward high frequencies; on the contrary, it is lower than expected if the total noise is spectrally located mainly at low frequencies.

Note that an enhanced resolution acquisition mode has also effect on the external noise, which is superimposed to the input signal. Such a beneficial effect should not be confounded with the ENOB improvement, which is attained by mitigating ADC quantization and imperfections and only refers to ADC non-idealities.

3. The proposed solution

Just as existing solutions do with baseband signals, the proposed built-in solution permits to improve the resolution in presence of band-pass signals by exploiting to the maximum the information on the signal spectral occupancy.

The proposed method can easily be built-in on board of DAS's, and is therefore quick, versatile and user-friendly. The idea is to perform a proper band-pass filtering capable of rejecting the part of quantization noise that is external to the band of analysis, including the noise located between the DC and the lower limit of such band. As an example, Fig. III-3 shows both the spectrum of a sinewave affected by uniform quantization noise and that of the same sinewave after that quantization noise has been partially rejected by means of band-pass filtering.

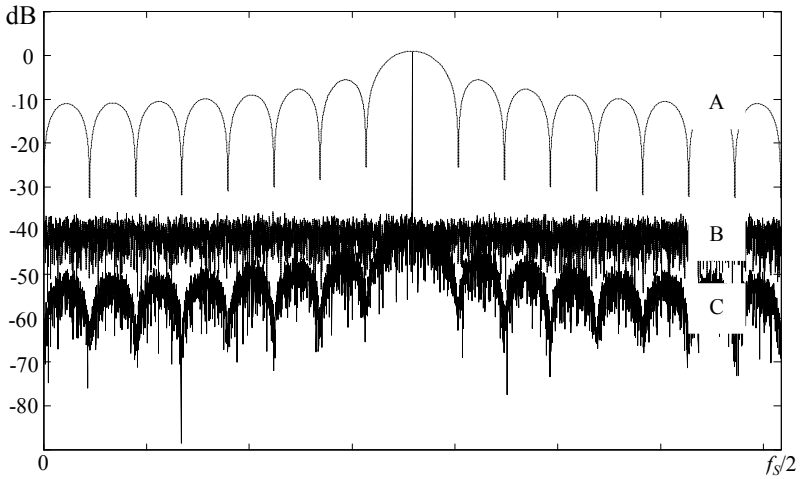

Fig. III-3: Improved resolution can be attained also in the presence of band-pass signals by means of a proper band-pass filter capable of rejecting the quantization noise external to the band of analysis. Three traces can be distinguished: the amplitude response of the filter (A), the spectrum of the sinewave affected by uniform quantization noise (B), and the spectrum of the same sinewave after band-pass filtering (C).

It is necessary to use a filter with linear phase response to avoid any distortions of the signal under test. To this end, a finite impulse response (FIR) filter should be preferred to an infinite impulse response (IIR) filter, which has poorer phase linearity. Actually, there exist advance filter design procedures that permit to design good IIR-filters [39],[40], but they are not the best choice for built-in solutions that require quickness of synthesis. Unfortunately, filter coefficients change according to the required low cut-off frequency and bandwidth. This is a major difficulty, because any firmware can only execute formerly-programmed control and processing operations. Presetting a limited set of different digital band-pass filters with constant parameters would be regarded as a misuse of firmware resources more than an additional facility, unlikely to meet up with every need.

A. Filter implementation and proposed hardware architecture

The proposed solution offers the possibility of acquiring the input signal and attaining the benefit of a digital band-pass filter effect.

Concerning the specific implementation, the proposed solution involves the storage of two mother sequences *MC* and *MS* representing, respectively, one cycle

of a cosine and of a sine function, into the ROM memory of the Control and Processing Unit of the DAS.

The samples of the two sequences are generated according to:

$$MC[n] = round\left[2^{b-1}\cos\left(\frac{2\pi}{M}n\right)\right],\ n = 0, \ldots, M\text{-}1 \tag{6}$$

$$MS[n] = round\left[2^{b-1}\sin\left(\frac{2\pi}{M}n\right)\right],\ n = 0, \ldots, M\text{-}1 \tag{7}$$

where *round* stands for the rounding operator, b is the number of bits of the adopted integer representation, and $M = 2^N$ is the length of the sequences.

The coefficients of the filter will be extracted from the two sequences that reside in the ROM, thanks to a pointer which is incremented, upon the acquisition of each new sample, of a suitable quantity Δ.

The algorithm inputs are: the sampling frequency f_s, and the spectral occupancy of the signal, in terms of its lower and upper spectral components (f_l and f_u). Its output is the quantity Δ, as well as the low cut-off frequency of the filter, *lcf* and the filter bandwidth B.

The filter bandwidth B can be selected among submultiples of 2 of the maximum sample frequency f_{SM} allowed by the DAS,

$$B = f_{SM}/2^q \tag{8}$$

where $2 \le q \le N\text{-}1$.

The iterative algorithm starts from the minimum value of $B = f_{SM}/2^{N-1}$ and increases it until it is greater than the signal bandwidth. The low cut-off frequency of the filter is chosen as

$$lcf = \left\lfloor \frac{f_l}{f_{SM}} M \right\rfloor \cdot \frac{f_{SM}}{M} \tag{9}$$

where $\lfloor\ .\ \rfloor$ returns the lower integer part.

The filter coefficients are then extracted from *MC* and *MS* thanks to a pointer *ptr*, which is defined as:

$$ptr = \mathrm{mod}_M\left(i \cdot \Delta\right) \tag{10}$$

where *mod* stands for the modulus operator, and Δ is the integer value, within $1 \leq \Delta \leq M \cdot 2^{q-1}$, obtained from (9) as

$$\Delta = \frac{lcf}{f_{SM}} M \ . \tag{11}$$

The pointer *ptr* is used for indexing and selecting specific elements from *MC* and *MS* at the occurrence of the generic *i*-th clock tick. Upon the increase of the index *i*, cosine and sine sequences represented by means of M/Δ points per cycle are extracted from *MC* and *MS* (see Fig. III-4).

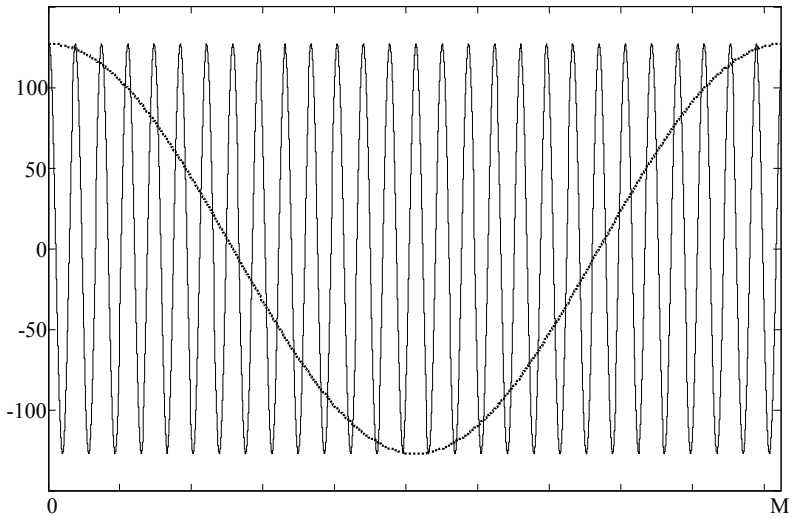

Fig. III-4: Cosine sequence characterized by a cycle length equal to $p \cdot 2^{N-q}$ extracted from *MC*. In this example $N = 10$, $M = 1024$, $\Delta = 36$.

It is worth noting that the filter coefficients are already stored in the ROM and do not need to be calculated each time. They are simply and quickly extracted from the ROM.

As an alternative, once the sampling frequency has been set, the user can choose the low cut-off frequency *lcf* and the bandwidth *B* of the filter from the list of values resulting from (8) and (9) upon the variation of q and Δ within their admitted range. Fig. III-5 gives examples of such selectable filters.

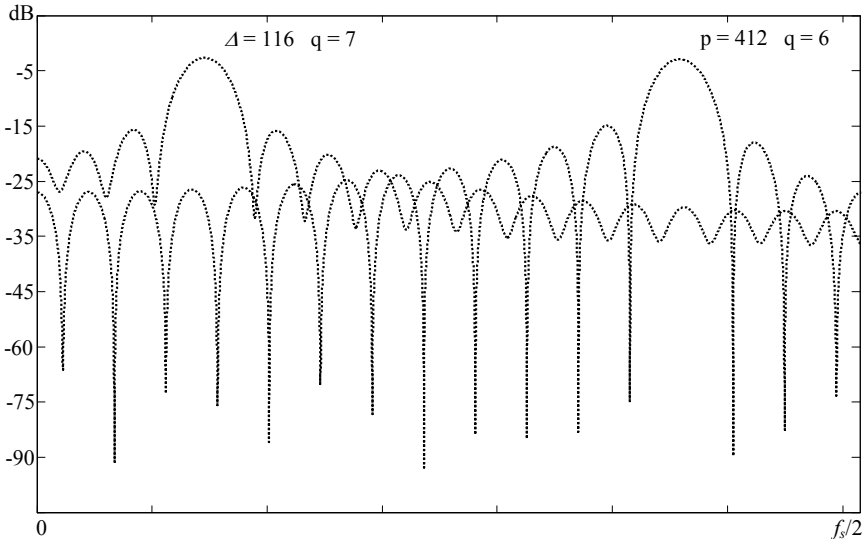

Fig. III-5: Amplitude response of two different filters that can be selected by the user (M = 1024). The band-pass filter that resides at lower center frequency is characterized by parameter values Δ = 116, and q = 7, while Δ = 412, and q = 6, for the other one.

Fig. III-6 gives a schematic view of the proposed solution. In particular, the figure shows the block diagram of the proposed filtering scheme, whereas Fig. III-7 depicts the implementation of the filter in the architecture of the control and processing unit of the DAS. The basic concept is a modulation (downconversion) of the input band-pass signal before a low-pass filtering (LPF) and a subsequent upconverson. The LPF is a moving average filter, whose intrinsic speed of operation makes it a suitable choice for the target built-in implementation in a high-speed DAS. The impulse response of the filter is

$$h(n) = \frac{1}{2^q} rect\left(\frac{n}{2^q}\right) \tag{12}$$

where rect(n/N) is a rectangular window of width N. It is easy to show that the upconversion-filtering-downconversion chain is equivalent to a band-pass filtering, with impulse response

$$h'(n) = \cos\left(2\pi\nu n\right) h(n) \ . \tag{13}$$

In fact, named X(ν) the DTFT (Discrete Time Fourier Transform) of $x(n)$, X_1(ν) and X_2(ν), which are the DTFT of $x_1(n)$ and $x_2(n)$ can be written respectively as:

$$X_1(\nu)=\frac{1}{2}\left[X(\nu-\nu_0)+X(\nu+\nu_0)\right]\cdot\frac{1}{2^q}\frac{1-e^{-j2\pi\nu 2^q}}{1-e^{-j2\pi\nu}} \tag{13a}$$

$$X_2(\nu)=\frac{1}{2j}\left[X(\nu-\nu_0)-X(\nu+\nu_0)\right]\cdot\frac{1}{2^q}\frac{1-e^{-j2\pi\nu 2^q}}{1-e^{-j2\pi\nu}} \tag{13b}$$

and the subsequent upconversion yields the following expression for $Y(\nu)$, the DTFT of $y(n)$

$$Y(\nu)=\frac{1}{2}X(\nu)\cdot\left[\frac{1}{2^q}\frac{1-e^{-j2\pi(\nu-\nu_0)2^q}}{1-e^{-j2\pi\nu-\nu_0)}}+\frac{1}{2^q}\frac{1-e^{-j2\pi(\nu+\nu_0)2^q}}{1-e^{-j2\pi\nu+\nu_0)}}\right] \tag{14}$$

which can be rewritten as

$$Y(\nu)=X(\nu)\cdot\left\{\frac{1}{2^q}\frac{1-e^{-j2\pi\nu 2^q}}{1-e^{-j2\pi\nu}}*\frac{1}{2}\left[\delta(\nu-\nu_0)+\delta(\nu+\nu_0)\right]\right\} \tag{15}$$

yielding to the following expression for the output sequence $y(n)$:

$$y(n)=x(n)*\left\{h(n)\cdot\cos(2\pi\nu_0 n)\right\} \tag{16}$$

Thus, the scheme in Fig.6a is equivalent to a band-pass filtering.

As regards the implementation (Fig. III-7), the data stream digitized by the ADC is duplicated and, at each clock tick, the *i*-th acquired sample and its duplicate are respectively multiplied by *MC*[*ptr*(*i*)] and *MS*[*ptr*(*i*)]. The results are then passed to two separate buffers, respectively *BC* and *BS*, which are managed according to the first-in-first-out (FIFO) logic rule. At each clock tick, the average value of the last $W = 2^q$ values flowing in *BC* and *BS* is returned and passed on (the length of the aforementioned buffer is related to the selected bandwidth *B*). The values coming out from *BC* and *BS* are multiplied, respectively, by *MC*[*ptr*(*i*-W)] and *MS*[*ptr*(*i*-W)]. Finally, the filtered sample is calculated as the sum of the results of the two multiplications.

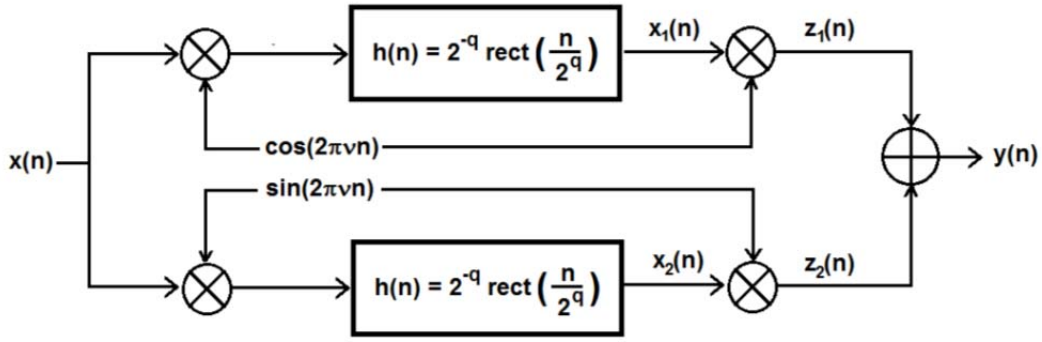

Fig. III-6: Block diagram of the filtering scheme.

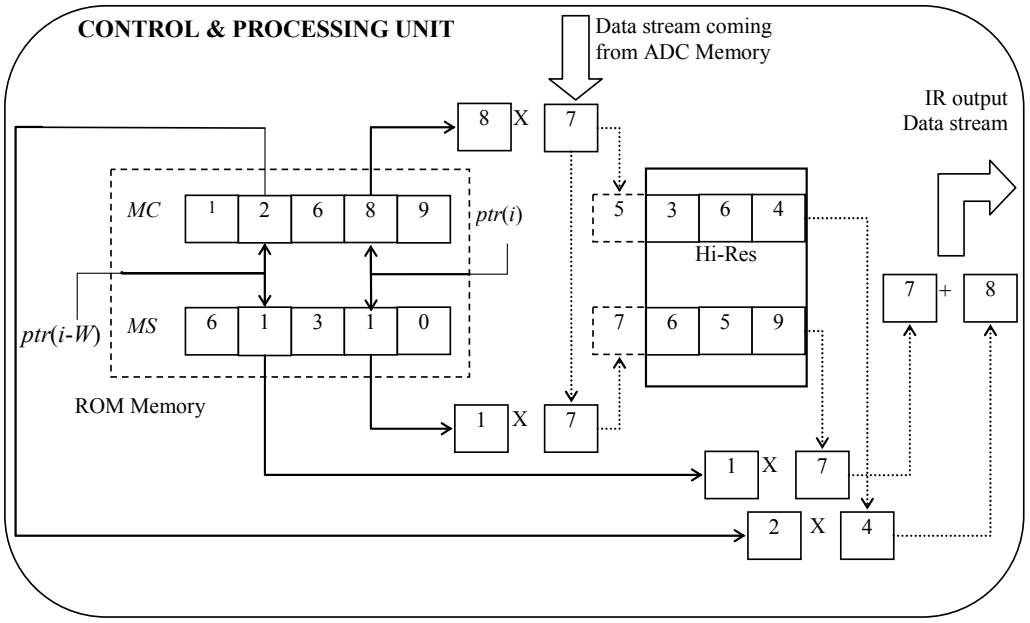

Fig. III-7: Schematic of the control and processing unit of the proposed DAS.

B. Resolution improvement

The proposed solution has two very interesting features: it has very little hardware requirements and allows acquiring a seamless data stream with improved resolution.

As regards the architecture, as shown in Fig. III-7, the processing only requires integer arithmetic and registers with enough bits to host the result without truncation, in order to prevent data truncation from deleting the improved resolution.

The theoretical resolution enhancement with respect to existing solutions can be evaluated for the proposed band-pass filtering similarly as it is done in (5), as

$$RE = \frac{1}{2}\log_2\left(\frac{f_S}{2B}\right). \tag{17}$$

Let us now compare the resolution improvement achievable with the proposed solution with that granted by the exiting filtering solution described in the above section. To do that, we need to calculate the difference ΔRE between the resolution improvements given in (5) and in (17):

$$\Delta RE = \frac{1}{2}\log_2\left(\frac{f_S}{2B}\right) - \frac{1}{2}\log_2\left(\frac{f_S}{2f_L}\right). \tag{18}$$

Let us assume that the band-pass signal has bandwidth B and carrier frequency f_c. Then, the cut-off frequency f_L appearing in (5) and (18) is equal to $f_c + B/2$, yielding

$$\Delta RE = \frac{1}{2}\log_2\left(\frac{f_c + B/2}{B}\right) \tag{19}$$

which can be rewritten as

$$\Delta RE = \frac{1}{2}\left[\log_2\left(1 + \frac{2f_c}{B}\right) - 1\right] \tag{20}$$

Expression (20) puts in evidence that the resolution improvement granted by the proposed solution, with respect to existing solutions, tailored for low-pass signals, is a function of the ratio f_c/B. In particular, ΔRE is a positive quantity, which is increased upon the increase of f_c/B. We could easily summarize this way: the more band-pass is the signal, the larger is the resolution improvement. Table III-1 gives the values of ΔRE achievable for some values of f_c/B.

4. Performance assessment

In order to assess the performance of the proposed acquisition mode, both simulations and experiments have been performed.

The metrics adopted to express the results are SINAD for the case of simulations and ENOB and SINAD for experiments.

Anytime it has been necessary to separate noise and signals, multiple linear regression algorithms, such as the well-known three parameters sine-fit algorithm, which represents a standard procedure for DAS characterization, have been exploited.

f_c/B	ΔRE
0.5	0
1	0.29
2	0.66
10	1.70
30	2.47
100	3.33
1000	4.98

Table III-1: Resolution enhancement granted by the proposed solution

A. Simulations

The signals adopted in the simulations are sinusoids corrupted by quantization and external noise. The addition of external noise allows having different values of SINAD for the test signals; all values are upper limited to the SINAD value of an 8-bit ideal DAS. All the results obtained through simulations show that the proposed acquisition mode improves the SINAD upon the narrowing of the selected bandwidth. The results are independent from the normalized frequency, *v,* of the signals, which has been always chosen within the interval (0.125, 0.375). Table III-2 gives the SINAD characterizing the signal acquired by means of the proposed acquisition mode, for different values of the SINAD characterizing the input signal and different values of the selected bandwidth, Δv, expressed in normalized units.

	SINAD of the input signal [dB]			
selected bandwidth, Δν	43.5	45.1	46.8	49.5
1/8	55.7	56.5	57.4	59.3
1/16	57.2	58.1	58.7	60.4
1/32	58.6	59.5	59.9	61.2
1/64	59.7	60.4	60.7	61.6
1/128	60.5	61.2	61.4	61.9

Table III-2: SINAD of the sinusoidal signal acquired by means of the proposed acquisition mode

In order to test the performance of the proposed acquisition mode in more challenging scenarios without losing the possibility of separating the signal power from the noise power by means of recognizable approaches, band-pass signals made up of two sinusoidal components have been considered. In the presence of periodic signals made up of a discrete number of sinusoidal components, the curve fitting problem can still be treated as a multiple linear regression problem. In particular, sinusoidal components with similar amplitudes have been considered; the bandwidth of the test signals is delimited by the frequencies of the components. The bandwidth of analysis is chosen in order to include the bandwidth of the input signal, as it is visible in Fig. III-8, which shows the amplitude spectra of the test signal (trace B) and its version obtained by means of the proposed acquisition mode (trace C). The reduction of the noise floor is clearly visible. The proposed acquisition mode produces the same effect of the band-pass filter shown with trace A. Table III-3 summarizes the results obtained in these simulations.

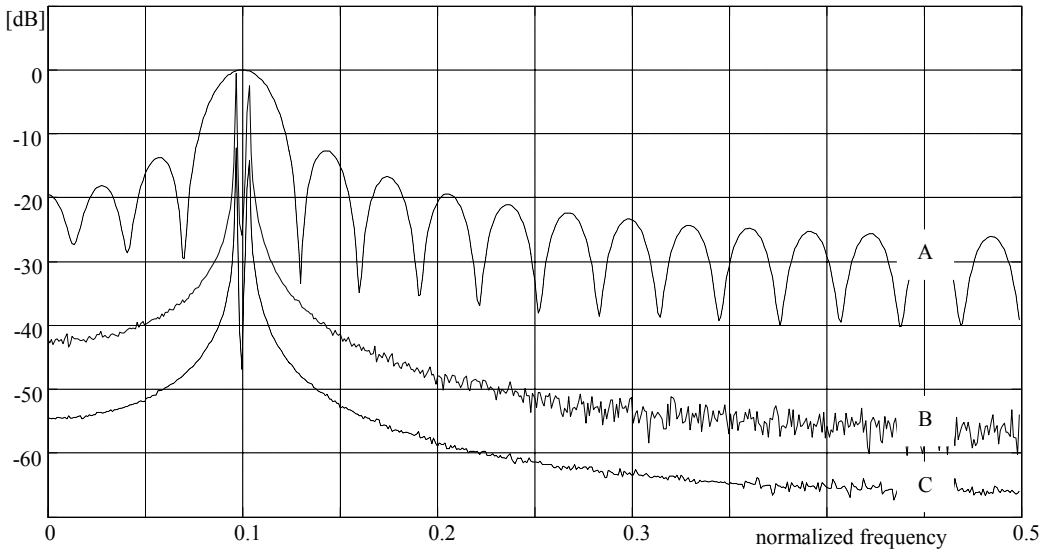

Fig. III-8: Amplitude spectra of the test signal (bold dash line) and its version obtained by means of the proposed acquisition mode (dot line). Trace (A) represents the filtering effect produced by the proposed acquisition mode.

	SINAD of the input signal [dB]			
selected bandwidth, Δv	44.2	45.6	46.7	48.6
1/8	56.5	57.0	58.0	58.9
1/16	57.7	58.3	59.4	59.9
1/32	59.1	60.0	60.8	61.4
1/64	60.2	61.0	61.7	62.1
1/128	61.7	61.7	62.6	62.9

Table III-3: SINAD of the signal made up of two sinusoidal components and acquired by means of the proposed acquisition mode

B. Experiments

In the experiments, a signal source and an 8-bit DAS characterized by maximum sample rate equal to 40 GS/s have been exploited. The ENOB and SINAD estimated on the data provided by the DAS and that estimated after the processing that implements the proposed acquisition mode have been compared.

Some tests with sinusoidal signals characterized by different frequencies have been performed. The signals have been acquired at a sample rate which is 1000 times higher than the frequency of the signal under test. The ENOB measured for the

adopted DAS ranges from 6.5 down to 6.2 bits when the frequency of the input signal increases from 1 kHz up to 1 MHz, and the sample frequency goes respectively from 1 MHz up to 1 GHz. Table III-4 gives the ENOB enhancement granted by the adopted DAS, for different choices of the acquisition bandwidth. The proposed data acquisition mode is capable of improving the ENOB almost up to 10.2 bits, when the selected bandwidth allows averaging 128 samples. In terms of SINAD it can be shown that the proposed acquisition mode grants enhancements upon the reduction of the selected acquisition bandwidth that range from 13.2 dB up to 15.1 dB for tests at 1 kHz, from 18.7 dB up to 22.9 dB for tests at 500 kHz, and form 18.7 dB up to 24.1 dB for tests at 1 MHz.

	Signal frequency [kHz]		
selected bandwidth	1	500	1000
fs/8	2.2	3.1	3.1
fs/16	2.4	3.4	3.5
fs/32	2.5	3.6	3.8
fs/64	2.5	3.7	3.9
fs/128	2.5	3.8	4.0

Table III-4: ENOB enhancement granted by the proposed acquisition mode

Signal characterized by two sinusoidal components have also been employed in the experiments. For instance, a signal made up of two components at frequencies 98.4 Hz and 101.6 Hz has been acquired using a sample rate equal to f_s = 1 kHz. The selection of a bandwidth equal to $B = f_s/64$ and centered at 100 Hz has assured an enhancement of 2.5 bits of ENOB, which is equal to an increase of 15.1 dB of SINAD.

Further experiments have been performed on frequency modulated signals. In particular, signals characterized by a sinusoidal frequency modulation have been acquired. By means of processing operations the versions produced by the proposed acquisition mode have also been determined. Both versions have been demodulated by means of a digital demodulator, which performs derivative and envelope detection. The SINAD of both demodulated waveforms has been

estimated in order to highlight the advantages obtained by means of the proposed acquisition mode. As an example, Fig. III-9 shows a portion of the amplitude spectrum of a frequency modulated signal characterized by a carrier frequency equal to 10 kHz, a modulation frequency equal to 100 Hz and a maximum frequency deviation equal to 500 Hz. In particular, the bold solid line represents the spectrum achieved by processing the data acquired by the DAS; the dotted line is instead the amplitude spectrum of the signal characterized by improved resolution. The sample frequency is f_s = 100 kS/s and a bandwidth equal to $f_s/8$ has been selected. The reduction of the noise floor is clearly visible. The proposed acquisition mode produces the same effect of the band-pass filter shown with the dash-dot line. The SINAD that characterizes the demodulated signal is 12.9 dB higher when demodulation is performed on the version acquired with enhanced resolution, rather than on that directly offered by the adopted DAS.

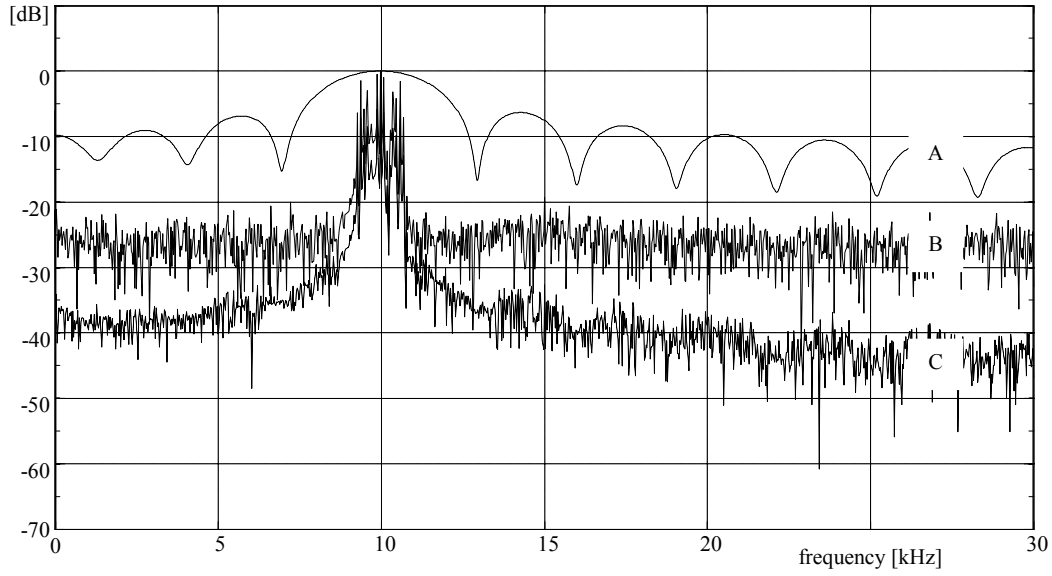

Fig. III-9: Amplitude spectra of the frequency-modulated signal under test (B) and its version obtained by means of the proposed acquisition mode (C). Trace (A) represents the filtering effect produced by the proposed acquisition mode.

IV. Analysis of Power Quality data

Since in power quality assessment harmonic analysis plays a key role, in this chapter modeling and analysis of the functioning of power systems in time varying conditions has been studied with the purpose of understanding how harmonic analysis could be used effectively in these scenarios. In particular the power systems have been described trough simplified approaches by recognizing load conditions that can be considered stationary within limited time intervals. A data segmentation approach to distinguish the time intervals in which stationary load conditions can be recognized has been proposed and assessed.

In detail, Section 1 both discusses the methods utilized to describe power systems, mainly based on the time domain harmonic source modeling, and highlights the applicative scenario for data segmentation approaches. Section 2 gives the theoretical details of the proposed segmentation algorithm. Section 3 shows the results of simulations carried out to assess the proposed algorithm.

1. Problem Statement

There are two widespread approaches to the modeling of electrical power system. When the attention is focused on the line impedance seen by the customer at the coupling point, the retrieved information is useful to assess the power quality that the customer can achieve. Whereas, when the attention is focused on the load in derivation from a point of common coupling (PCC), the retrieved information should help the provider in charging specific customers with the responsibility of the harmonic pollution.

Nowadays, because of distributed generation, there can be bidirectional power flows in power systems, therefore modeling of loads and line impedance has to change with respect to past years. In particular, loads linked at a PCC have to be schematized as shown in Fig. IV-1, where Z_{in}, E_{in} represent the Thevenin equivalent parameters of the power supply, and loads of different nature can be enlisted. Connecting and/or disconnecting the various loads determine different

network configurations as well as different load conditions. Furthermore, even if the network configuration keeps unchanged, inherent load variations can occur and change load conditions.

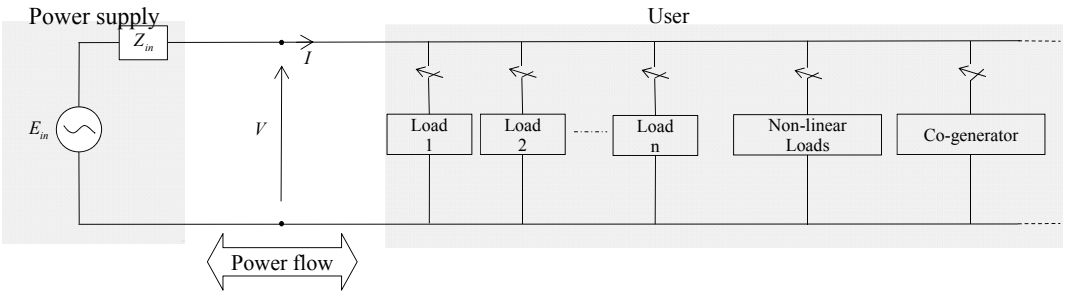

Fig. IV-1: Generic network configuration: loads can be of different nature.

For time intervals in which load conditions appear almost homogenous, with voltages and currents having a stationary power spectrum, a Norton equivalent circuit can be used as shown in Fig. IV-2 to describe each load. In Fig. IV-2 $\dot{Z}_{eq}(f)$ is the equivalent impedance and $\dot{I}_{NL}(f)$ is the current source taking into account the non-linear current that the load injects in the power system.

Applying the Fourier theorem, voltage and current can be decomposed as the sum of harmonics:

$$\begin{aligned} \dot{V}(f) &= \dot{V}(f_1) + \sum_{h=2}^{+\infty} \dot{V}(h \cdot f_1) = \dot{V}_{[1]} + \dot{V}_{[H]} \\ \dot{I}(f) &= \dot{I}(f_1) + \sum_{h=2}^{+\infty} \dot{I}(h \cdot f_1) = \dot{I}_{[1]} + \dot{I}_{[H]} \end{aligned} \tag{1}$$

where f_1 is the fundamental frequency.

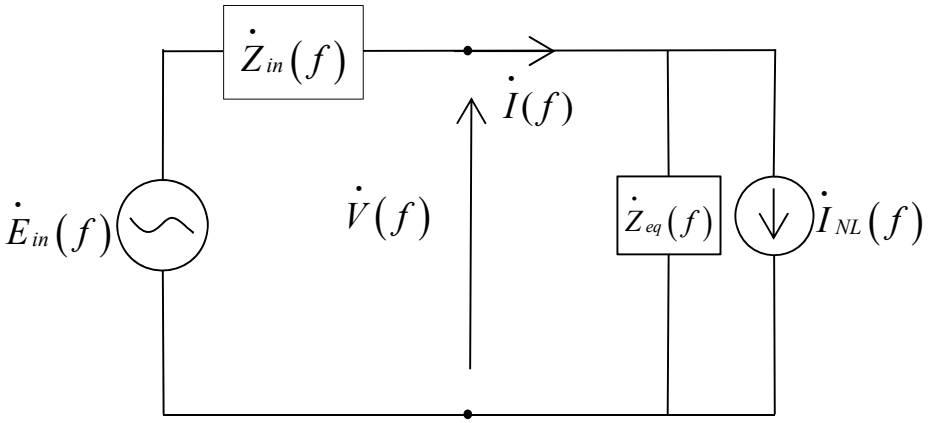

Fig. IV-2: Equivalent circuit of the power system to be considered in a limited period of time in which the current related to a load has a stationary power spectrum.

Note that the line impedance plays a crucial role in the propagation of harmonic pollution. Since the supply and the line connecting loads have a non-negligible impedance, the voltage measured at a PCC is not purely sinusoidal because of the voltage drops due to the harmonic currents injected by the non-linear loads:

$$\begin{aligned} \dot{V}(f) &= \dot{E}_{in}(f) - \dot{Z}_{in}(f)\dot{I}(f) = \dot{V}_{[1]} + \dot{V}_{[H]} \\ \dot{I}(f) &= \dot{I}_{[1]} + \dot{I}_{[H]} \end{aligned} \tag{2}$$

Fig. IV-2 also describes the Thevenin equivalent circuit of the supply seen by a generic load. The parameters of the circuit in this case are different both for each harmonic and for each of the different coupling points that can be considered in the network. The harmonic pollution produced by a load affects the quality of the voltage of all the other loads that share the same network. When the coupling point is immediately at the output of the generator, the line impedance instead coincides with the inherent impedance of the generator and the voltage generator can be approximated with a short circuit at all harmonics except the fundamental frequency.

Applying Kirchhoff's voltage law to the equivalent circuit in Fig. IV-3 at the harmonic order h^{th}, it holds:

$$\dot{V} = \dot{E}_{in} - \dot{Z}_{in}\dot{I} \tag{3}$$

(to simplify the mathematical notation the harmonic order has not been highlighted). The complex equation (3) cannot be solved because there are two complex unknowns. At least two couples of independent equations are needed to solve the problem and evaluate the parameters. If a second equation can be written the solution is given by:

$$\begin{cases} \dot{Z}_{in} = \dfrac{\dot{V}_1 - \dot{V}_2}{\dot{I}_2 - \dot{I}_1} \\ \dot{E}_{in} = \dot{V}_1 + \dot{Z}_{in}\dot{I}_1 \end{cases} \tag{4}$$

In fact, as well known, the parameters of a Thevenin equivalent circuit must be determined measuring the circuit in two different load conditions. It is worth noting that measurements repeated in the same stationary condition do not provide sufficient information to solve (4) since they fictitiously differ because of the action of the uncertainty sources.

Two different approaches, which can be distinguished between invasive and non-invasive, are usually deployed to face the aforementioned problem [52-53]. The invasive approach deploys specifically designed equipment, such as saturated transformers or switching capacitors, to modify load conditions and inject harmonic currents in the neutral connection. This is an invasive method because for measurement purposes loads that are absent in the network during the normal functioning are connected and activated. When recurring to the non-invasive approach, measurements are carried out before and after natural variations of the power system. A statistical method for the recognition of natural variations can be used to select the different load conditions. An example of the aforementioned method is presented in [53]. In particular, the method is based on the division of the entire time of interest into sufficiently small sub-intervals, according to the time aggregation concept introduced by the IEC Standard 61000-4-30. Measurements of voltage and current are performed in each sub-interval. Then a least square algorithm is used to determine the solution of the over-determined system of equations obtained. Starting from this set of determinations, a

probability function of the unknown parameters is built up in order to find the statistic assessment.

In this work a different non-invasive method to characterize the network and evaluate the power quality that a customer can rely on is proposed. It is mainly based on a preliminary data segmentation processing to distinguish different load conditions that lead to independent equations.

In fact considering the generic m^{th} load condition, and the successive $(m+1)^{th}$ one, the (4) becomes:

$$\begin{cases} \dot{Z}_{in} = \dfrac{\dot{V}^{[m]} - \dot{V}^{[m+1]}}{\dot{I}^{[m+1]} - \dot{I}^{[m]}} \\ \dot{E}_{in} = \dot{V}^{[m]} + \dot{Z}_{in}\dot{I}^{[m]} \end{cases} \tag{5}$$

The parameters in (5) have to be correctly interpreted. In fact, except for the case in which they are related to the coupling point immediately at the output of the generator, they represent the average value of the parameters of two different equivalent Thevenin circuits. These two circuits represent the line seen by the customer during two consecutive time intervals characterized by different stationary conditions.

Considering the time instants at which load conditions change, for each time instant an estimate of the parameters can be given. The time domain evolution of the considered parameters can be reconstructed starting from the collection of the estimates, which represent a non-uniformly sampled time data trend. These data trend can be useful to statistically characterize the electrical network.

2. data-segmentation algorithm

A. Introduction

The recognition of the different operating conditions is gained by means of data segmentation algorithms, which are applied to the line current values measured at a given sample rate. The collected line current measurements are usually average values within time intervals including several cycles of the waveform, ranging

from fractions of seconds to some minutes. These measurements are performed within very long time intervals, which include several days or weeks, and are precious to investigate the differences between load conditions during daily working hours, as well as at night and week-end.

In the practice, two data segmentation algorithms are principally utilized to recognize different load conditions [50]. The first algorithm uses a standard deviation estimate of the root mean square value of the line currents to the purpose. In detail, all the acquired record containing the line current values is first separated into short subsets of pre-selected length; the sample standard deviation characterizing each subset is then estimated and compared to a threshold; if the threshold is overcome, the subset reveals that the load conditions have changed during the time interval the subset is related to. When adopting this algorithm, however, the user should be acquainted that the sample standard deviation has to be estimated by means of the proper formula according to the length of the considered subset: if the subset counts a few samples it would be better to derive an estimate of the sample standard deviation as percentage of the sample range. In this case, in fact, the use of the common formula for sample standard deviation, which takes into account the root mean square deviations, would mislead load conditions classification, since the obtained results have week relation with data dispersion.

The second algorithm distinguishes different load conditions by analyzing the slope of the time domain evolution of the root mean square value of the line current. When the system moves from a given load condition to a different one, the line current is characterized by a significant step.

A. Proposed *algorithm*

A new data segmentation algorithm to evaluate different load conditions is hereafter proposed. The algorithm is based on the use of a moving average filter for estimating the value of the current, which is representative of the load conditions. At each step of the analysis the current value is compared to the average value obtained by means of the aforementioned filter in order to verify if

the difference between them exceeds or not a given threshold. If the threshold is not overcome the average value is updated. On the contrary, the current sample will be the first one of a new segment, and at the next processing step will be used to judge the incoming current value. The threshold value is pre-assigned as a given percentage of the aforementioned average current value.

In detail, let us consider the values of the current measured at PCC collected into the set *I*:

$$I = \{I_1; I_2; I_3; \cdots I_N;\} \tag{6}$$

Let us also assume that the first $k-1$ samples have been judged, and all belong to the same time interval in which the load conditions can be considered stable. At step $(k-1)^{th}$, the average value of the current is equal to:

$$< I >_{k-1}^{[l]} = \frac{1}{k-1}\sum_{n=1}^{k-1} I_n \tag{6}$$

At next step *k*, the distance of the value of the current I_k with the average one, $< I >_{k-1}^{[1]}$ at the step $k+1$, is estimated and compared to a dynamically varying threshold, which is a given percentage of the average, extracted by means of coefficient α. If it occurs that:

$$\frac{\left| I_k - < I >_{k-1}^{[1]} \right|}{< I >_{k-1}^{[1]}} < \alpha \tag{7}$$

An updated average value is calculated including the new sample, namely:

$$< I >_{k}^{[1]} = \frac{(k-1) < I >_{k-1}^{[1]} + I_n}{k} \tag{8}$$

If inequality (8) is not satisfied the sample I_k is judged as the initial point of a second segment, representative of a separate time interval in which different load conditions take place. A new reference average value is estimated according to:

$$< I >_1^{[2]} = I_k \tag{9}$$

Moreover it can be recorded that the previous segment has length $l_1 = k - 1$

In general, let us consider the generic segment *m*. The total number of samples included in the segments up to $m-1$ is equal:

$$L_{m-1} = \sum_{j=1}^{m-1} l_j \tag{10}$$

where l_j is the length of the segment *j*.

The average value of the current related to the segment *m* at the step $k-1$ is equal to:

$$< I >_{k-1}^{[m]} = \frac{1}{k-1} \sum_{n=1}^{k-1} I_{L_{m-1}+n} \tag{11}$$

At next step, the distance of the value of the current $I_{k+L_{m-1}}$ with the average one $< I >_{k-1}^{[m]}$, is estimated and compared to the related threshold as follow:

$$\frac{\left| I_{k+L_{m-1}} - < I >_{k-1}^{[m]} \right|}{< I >_{k-1}^{[m]}} < \alpha \tag{12}$$

If inequality (13) is satisfied, an updated average value is calculated including the new sample, namely:

$$< I >_k^{[m]} = \frac{(k-1) < I >_{k-1}^{[m]} + I_{k+L_{m-1}}}{k} \tag{13}$$

Meanwhile, if inequality (13) is not satisfied the sample $I_{k+L_{m-1}}$ is judged as the initial point of the next segment $(m+1)^{th}$ Also a new reference average value is estimated according to:

$$< I >_1^{[m+1]} = I_{k+L_m} \tag{14}$$

The proposed segmentation algorithm shows some interesting performance in terms of both robustness and capability of highlighting load conditions characterized by short duration, which are instead not detected and included into adjacent time intervals related to load conditions of longer duration by the other approaches

Furthermore, the proposed approach has low computational burden; thus it can be easily implemented in order to have real time segmentation.

3. Performance assessment

To assess the performances of the proposed algorithm several interesting situations are considered.

First, it is worth noting that the choice of the threshold is a critical issue. The current segmentation strictly depends from the threshold choice. The reasoning for selecting a threshold that slightly varies with the average value of the current derives from the analysis of typical scenarios. In particular, the current variability seems proportional to the magnitude of the average current in the time interval related to homogeneous load conditions.

An interesting situation is related to the case of currents that constantly increase with time. Although the average value is updated at each new processed sample and exhibits an increment, this increment is not constant but becomes smaller and smaller as the number of averaged measurements increase. Thus, even if the threshold value is affected by the underground increments, the distance between the new sample and the average value in the presence of a constant slope in the long run overcomes the threshold. The processed data correctly highlights different load conditions as shown in Fig. IV-3, without needing further controls to notice the slowly constant data variation.

Another special situation occurs in the presence of temporarily load conditions of short duration, which are revealed by very short sequences or at last by isolated points. Processing should not treat the values of very short sequences or isolated points as noisy effects; it should rather detect the temporarily load condition as a

specific one and highlight the presence of a segment with short length. The effect of noise is in fact effectively mitigated by the average processing, which is inherent in the monitoring itself.

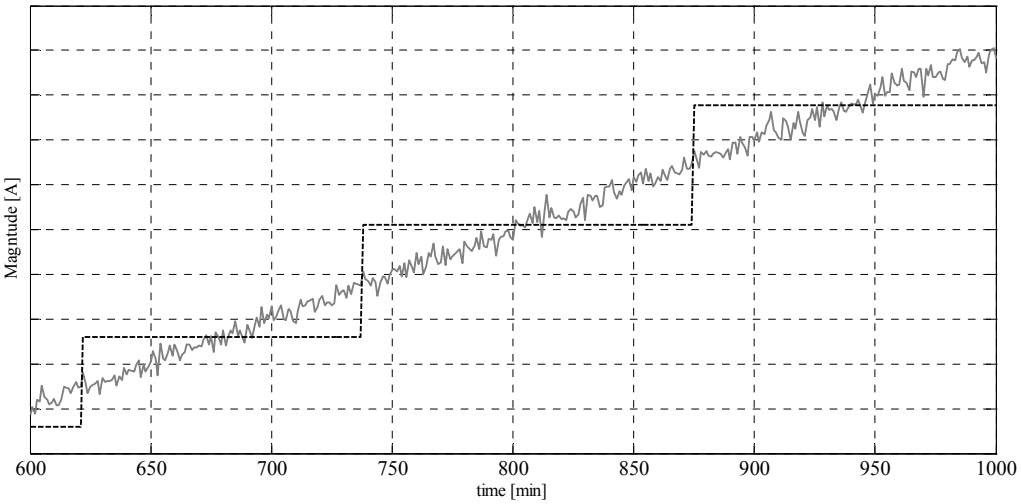

Fig. IV-3: Data characterized by a continuous slow increment and segmentation results obtained by means of the proposed algorithm (dash line)

Tests to simulate the aforementioned situations have been performed. In a first test the adopted test sequence is made up of different constant subsequences linked in series, which provide a piecewise frame, to which small random deviations are superimposed. The different load conditions are related to the different average values that characterize the underlying piecewise evolution of the test sequence. The deviations with respect to the average values are limited to a given percentage of the same aforementioned average value: heavy load conditions are characterized by larger data fluctuations with respect to light load conditions. Furthermore some isolated points are included in the same test signal considered in order to simulate the presence of very short temporarily load conditions. An example of test sequence in which four different consecutive load conditions have been simulated is shown in Fig. IV-4.

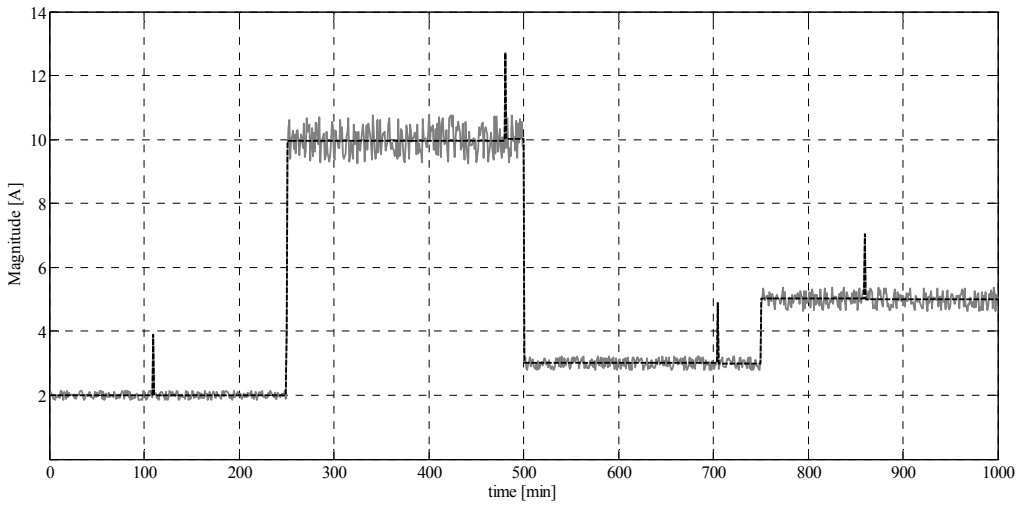

Fig. IV-4: Simulated test signal (solid line) and segments extracted by the proposed algorithm (dash line).

The results obtained by applying the proposed algorithm to the test sequence given in the figure accurately recognize the different load conditions even highlighting the presence of load conditions of very short duration.

The proposed approach has been tested also in the presence of real data. In particular, data related to the line currents at the output of a MV/LV substation wye-connected have been recorded. The data consist in the average values of the RMS and harmonic contributions sampled any 10 minutes by means of a power quality analyzer (Fluke 1760); the observed period ranges from July 29th to September 2nd, 2011. A portion of the recorded data is shown in Fig. IV-5; here the time domain evolution of the current of a single phase is shown; the observed time period is about fifteen days: the different load conditions between daily working hours and night and week-end are clearly visible. In particular, the electrical system as expected appears less loaded during the week end and the night being the absorption typically below 80 A, while it is more loaded and can increase up to 150 A during daily hours.

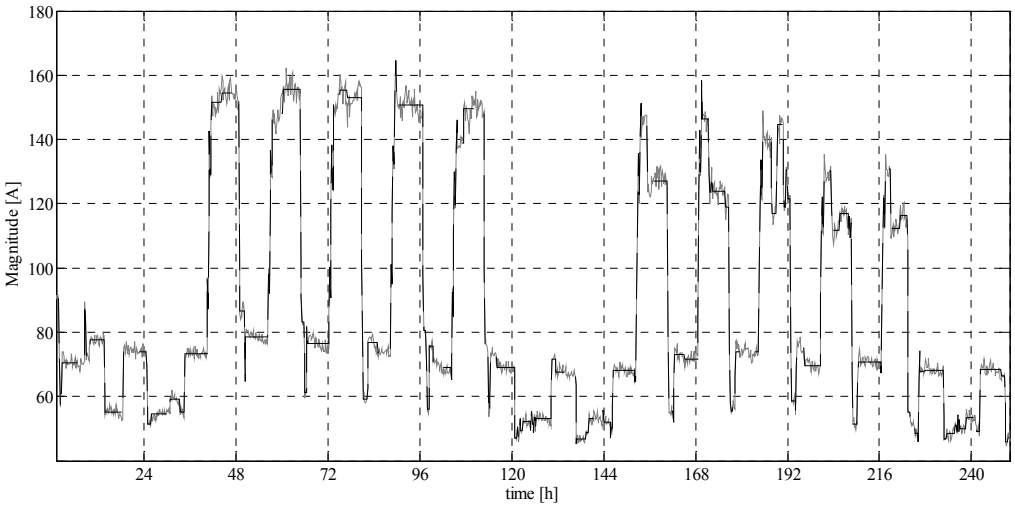

Fig. IV-5: Segmentation results related to experimental data of the current, 10-minute averaged.

V. Conclusion

In this work several important aspects of power quality are discussed, and measurement methods aimed at disturbances detection are proposed.

In order to investigate the effects of poor power quality on electrical equipment, in particular on measurement instrumentation, susceptibility studies have been carried out considering the disturbances referred into standard CEI EN 50160. Controlled power quality disturbances have been injected in instrumentation and both reliability and accuracy issues have been checked in the tests.

A second aspect taken into account is that related to the instrumentation needed for the analysis of the power quality. So aspects of the implementation of a low-cost, microcontroller-based, distributed network analyzer have been discussed. The implemented system has been developed in respect of IEC 61000-4-30 constraints. The implemented multi-analyzer is capable of measuring the power quality disturbances of individual users and to communicate with decentralized control unit through the CAN bus, which has the option to remotely monitor the activities of the devices connected to the system. The control unit includes a web server that allows to collect the statistics of power consumptions and power quality events. Characterization tests of realized apparatus have shown good performances both in terms of communication errors and measurement uncertainty.

Several details related to suitable strategies to increase measurement resolution have also been considered. In particular a proposal for a data acquisition system architecture with built-in resolution enhancement functionalities optimized for band-pass signals has presented. The solution extends the idea of oversampling and subsequent filtering which is behind the enhanced resolution techniques available on top-level general purpose

DAS's. Besides giving the design and algorithmic details of the proposed solution, an analytical comparison of the resolution improvement with respect to existing enhanced resolution improvement techniques, as well as the results of several simulative and experimental tests for the performance assessment are given. The reduction of the noise floor is clearly visible from the experimental results. The proposed acquisition mode produces the same effect of the band-pass filter: in terms of SINAD the proposed acquisition mode grants enhancements of even more than 10 dB, depending on the band-pass nature of the test signal. An important feature is that this solution shows efficient in terms of hardware requirements and processing time.

Finally, since in power quality assessment harmonic analysis plays a key role, modeling and analysis of the functioning of power systems in time varying conditions has been studied with the purpose of understanding how harmonic analysis could be used effectively in these scenarios. Thus a time-domain harmonic source model is considered to describe loads in power systems, and a new data segmentation algorithm to detect different load conditions in power systems has been proposed. The proposal is based on the assumption that once the current is stationary in a period of time, harmonic impedance and voltage source during this period of time can be viewed stationary as well. In the proposal a moving average has been used to separate acquired data in several segments in which the current can be considered stable. Each segment represents a load condition. To analyze its effectiveness, the proposed algorithm has been tested with simulation and in the presence of experimental data.

VI. References

[1] B. D'Apice, C. Landi, A. Pelvio, N. Rignano - A multi-DSP based instrument for real-time energy and PQ measurements Metrology and Measurement Systems, p. 495, VOL. XIV, NUMBER 4 (2007)

[2] Minosi, A.; Martinola, A.; Mankan, S.; Balzarini, F.; Kostadinov, A.N.; Prevostini, A.; "Intelligent, low-power and low-cost measurement system for energy consumption", Virtual Environments, Human-Computer Interfaces and Measurement Systems, 2003. VECIMS '03. 2003 IEEE International Symposium on, Publication Year: 2003 , Page(s): 125 – 130

[3] McEachern, A.; Eberhard, A.; "A new, ultra low cost power quality and energy measurement technology - the future of power quality monitoring", Power Systems Conference and Exposition, 2009. PSCE '09. IEEE/PES, Publication Year: 2009 , Page(s): 1 - 4

[4] IEC EN 50160, "Voltage characteristics of electricity supplied by public distribution systems", CENELEC, 1999.

[5] Mo Guan; Minghai Gu, "Design and Implementation of an Embedded Web Server Based on ARM",Software Engineering and Service Sciences (ICSESS), 2010 IEEE International Conference on Digital Object Identifier; 16-18 July 2010.

[6] IEEE Task Force P1159.1: Guide For Recorder and Data Acquisition Requirements for Characterization of Power Quality Events, Draft 1.8 January 2004.

[7] IEC Standard IEC 61000-4-30, Testing and measurement techniques – PQ measurement methods, 2003-11

[8] D.Gallo, C.Landi, N.Rignano, "Multifunction DSP based real-time power quality analyzer", XVIII IMEKO World Congress Metrology for a sustainable development. Septmber, 17-22, 2006. Rio de Janeiro, Brazil.

[9] Wu Min-hua, "Research for the Embedded WEB Server", Coll. of Inf. Eng., Capital Normal Univ., Beijing; Microwave Conference, 2008 China-Japan Joint; 10-12 Sept. 2008.

[10] D. Gallo, G. Ianniello, C. Landi, M. Luiso, "An advanced energy/power meter based on ARM microcontroller for smart grid applications"., Second University of Naples; 17th Symposium IMEKO TC 4, 3rd Symposium IMEKO TC 19 and 15th IWADC Workshop Instrumentation for the ICT Era; Sept. 8-10, 2010, Kosice, Slovakia.

[11] F. Ciancetta, B. D'Apice, D. Gallo, C. Landi, "Architecture for Distributed Monitoring based on Smart Sensor and Web Service", IMTC2006 – Instrumentation and Measurement Technology Conference Sorrento, Italy, 24-27 April 2006.

[12] F. Ciancetta, E. Fiorucci, B. D'Apice, C. Landi "A Peer-to-Peer Distributed System for Multipoint Measurement Techniques" Proceedings of IEEE Instrumentation and Measurement Technology Conference, Warsaw, Poland, May 1-3, 2007.

[13] Kang Lee and Eugene Song "Smart Transducer Web Services Based on the Proposed IEEE 1451.0 Standard", Proceedings of IEEE Instrumentation and Measurement Technology Conference, Warsaw, Poland, May 1-3, 2007.

[14] IEC Standard EN 61000-4-7; Testing and measurement techniques - General guide on harmonics and interharmonics measurements and instrumentation, for power supply systems and equipment connected thereto, 2003-07

[15] C. Liguori, V. Paciello, A. Paolillo, A. Pietrosanto, 'Improving and qualifying spectrum analysis made by digital scopes,' IEEE Trans. on Instr. and Meas., Vol. 56, No.6, Dec. 2007, pp.2411-2419.

[16] Tektronix Application Note 55W-17443-2, TDS5000B, TDS6000B, TDS/CSA7000B Series Acquisition Modes,

http://www2.tek.com/cmsreplive/tirep/2305/55W_17443_2_2009.04.14.10.11.57_2305_EN.pdf [online].
[17] LeCroy Application Note AN006A, "Enhanced Resolution", http://www.lecroy.com/files/AppNotes/AN_006a.pdf [online].
[18] L. Angrisani, M. D'Arco, M. Vadursi, "Error Vector-Based Measurement Procedures for RF Digital Transmitters Troubleshooting," IEEE Trans. on Instrumentation and Measurement, vol.54, No.4, Aug. 2005, pp.1381-1387.
[19] L. Angrisani, M. D'Arco, M. Vadursi, "Clustering-based Method for Detecting and Evaluating I/Q Impairments in Radio Frequency Digital Transmitters," IEEE Trans. on Instr. and Meas.., vol.56, No.6, Dec. 2007, pp. 2139-2146.
[20] L. Angrisani, I. Ghidini, M. Vadursi, "A New Method for I/Q Impairment Evaluation in OFDM Transmitters," IEEE Trans. on Instr. and Meas., vol.55, No.5, pp.1480-1486, Oct. 2006.
[21] S. Caban, A. Disslbacher-Fink, J. A. García Naya, M. Rupp, "Synchronization of wireless radio testbed measurements," Proc. of IEEE Intern. Instr. and Meas. Tech. Conf I2MTC 2011, pp. 1-4, 10-12 May 2011.
[22] S. Caban, J. A. García Naya, M. Rupp, "Measuring the Physical Layer Performance of Wireless Communication Systems," IEEE Instr. and Meas. Magazine, vol.14, No.9, pp. 8-17, Oct. 2011.
[23] L. Noel, P. Brousse, "Low-Cost EVM Test Methodology for Wireless Transmitters Applied to W-CDMA," IEEE Trans. on Instr. and Mea,s vol.60, no.1, pp.170-175, Jan. 2011.
[24] L. Angrisani, A. Napolitano, M. Vadursi, "Measuring I/Q Impairments in WiMAX Transmitters," IEEE Trans. on Instr. and Meas., vol.58, No.5, pp. 1299-1306, May 2009.
[25] L. Angrisani, M. D'Arco, M. Vadursi, "Modulation Tests on Bluetooth Transmitters Through Time-Frequency Representations," IEEE Trans. on Instr. and Meas., vol.56, No.6, pp. 2147-2154, Dec. 2007.
[26] L. Angrisani, M. D'Apuzzo, M. Vadursi, "Power Measurement in Digital Wireless Communication Systems through Parametric Spectral Estimation," IEEE Trans. on Instr. and Meas., vol.55, No.4, pp.1051-1058, Aug. 2006.
[27] R.G. Vaughan, N.L. Scott, D.R. White, "The theory of bandpass sampling," IEEE Trans. Signal Proc., vol. 39 pp.1973–84, 1991.
[28] C. H. Tseng, "Bandpass sampling criteria for nonlinear systems," IEEE Trans. Signal Process., vol. 50, pp.568–77, 2002.
[29] F. Stefani, D. Macii, A. Moschitta, P. Carbone, D. Petri, "A Simple and Time-effective Procedure for ADC INL estimation", IEEE Trans. on Instr. and Meas., Vol. 55, n. 4, pp. 1383-1389, Aug. 2006.
[30] G. Betta, D. Capriglione, L. Ferrigno, G. Miele, "Innovative methods for the selection of bandpass sampling rate in cost-effective RF measurement instruments," Measurement, Vol. 43,No. 8, pp. 985–993, Oct. 2010.
[31] L. Angrisani, M. D'Arco, C. Greenhall, R. Schiano Lo Moriello, "Optimal bandpass sampling strategies for enhancing the perfoemance of a phase noise meter," Meas., Sci. and Tech., vol.19, n.10, pp.1-11, Aug. 2008.
[32] L. Angrisani, M. D'Arco, C. Greenhall, R. Schiano Lo Moriello, "A digital signal processing instrument for real-time phase noise measurements," IEEE Trans. on Instr. and Meas., Vol. 57, n. 10, pp. 2098-2107, Oct. 2008.

[33] L. Angrisani, M. Vadursi, “On the optimal sampling of bandpass measurement signals through data acquisition systems,” Meas., Sci. and Tech., vol.19, n.4, pp.1-9, Apr. 2008.
[34] L. Angrisani, M. D’Arco, G. Ianniello, M. Vadursi, “Novel built-in solution for data acquisition system resolution enhancement,” Proc. of IEEE Intern. Instr. and Meas. Tech. Conf. I2MTC/11, May 10-12, 2011, Hanghzhou, China, pp. 1783-1787.
[35] V. Haasz, J. Roztocil, D. Slepicka, “Evaluation of ADC testing systems using ADC transfer standard,” IEEE Trans. on Instr. and Meas., Vol. 54 , No. 3, pp. 1150 – 1155, June 2005.
[36] A. C. Serra, M. F. da Silva, P. M. Ramos, R. C. Martins, L. Michaeli, J. Saliga, “Combined spectral and histogram analysis for fastADC testing,” IEEE Trans. on Instr. and Meas., Vol. 54 , No. 6, pp. 1617 – 1623, June 2005.
[37] IEEE Std 1241™-2010: IEEE Standard for Terminology and Test Methods for Analog-to-Digital Converters, 14 January 2011.
[38] W. A. Kester, “The Data Conversion Handbook,” Elsevier, 2005.
[39] R. Vuerinckx, Y. Rolain, J. Schoukens, R. Pintelon, ”Design of stable IIR filters in the complex domain by automatic delay selection,” IEEE Trans. on Signal Proc., Vol. 44, No. 9, pp. 2339-2344, Sep. 1996.
[40] R. Vuerinckx, Y. Rolain, “Design of a Very High-Resolution Network Analyser,” Proc. of Instr. and Meas. Tech. Conf. IMTC/93, May 18-20, 1993 Irvine, CA, pp. 470-475.
[41] J. Ma, D.J. Hill, Z. Y. Dong, R. M. He, “Power system energy analysis incorporating comprehensive load characteristics ,” IET Gener. Transm. Distrib. (2007), Vol. 1, N. 6, pp. 855-863.
[42] Y. Baghzouz, R. F. Burch, A. Capasso, A. Cavallini, A. E. Emanuel, M. Halpin, A. Imece, A. Ludbrook, G. Montanari, K. J. Olejniczak, P. Ribeiro, S. Rios-Marcuello, L. Tang, R. Thaliam, P. Verde, “Time-varying harmonics. I. Characterizing measured data”, IEEE Transactions on Power Delivery, Jul 1998, vol. 13, N. 3, pp.938-944.
[43] Lok-Fu Pak; V. Dinavahi, Gary Chang, M. Steurer, P. F. Ribeiro, “Real-Time Digital Time-Varying Harmonic Modeling and Simulation Techniques”, IEEE Trans. On Power Delivery, April 2007, vol. 22, N. 2, pp.1218-1227.
[44] Chang, G., "Characteristics and Modeling of Harmonic Sources-Power Electronic Devices", IEEE Power Engineering Review, Aug. 2001, vol. 21, N. 8, pp. 62-63.
[45] P. F. Ribeiro, “A novel way for dealing with time-varying harmonic distortions: the concept of evolutionary spectra,” IEEE Power Engineering Society General Meeting, July 2003, vol. 2, N. 4, pp. 13-17.
[46] G. D'Antona, C. Muscas; P. A. Pegoraro, S. Sulis, "Harmonic Source Estimation in Distribution Systems", IEEE Transactions on Instrumentation and Measurement, Oct. 2011, Vol. 60, N. 10, pp. 3351-3359.
[47] M. Farhoodnea, A. Mohamed, H. Shareef, “A new method for determining multiple harmonic source locations in a power distribution system” IEEE International Conference on Power and Energy, Dec. 2010, pp.146-150.
[48] IEEE Task Force on Harmonic Modeling and Simulation, “Modeling and simulation of the propagation of harmonics in electric power systems part I: Concepts, models, and simulation techniques”, IEEE Transactions on Power Delivery, Jan. 1996, Vol. 11, N. 1, pp. 452–464.
[49] M. D’Apuzzo, M. D'Arco, “A time-domain approach for the analysis of non-stationary signals in power systems”, IEEE Transactions on Instrumentation and Measurement, Vol.57, N. 9, Sept. 2008, pp. 1969-1977.

[50] W. Li, Y. Wang, T. Chen, "Investigation on the Thevenin equivalent parameters for online estimation of maximum power transfer limits," IET Gener. Transm. Distrib. (2010), Vol. 4, N. 10, pp. 1180-1187.
[51] M. Dong, H. E. Mazin, W. Xu "Data segmentation algorithms for a time-domain harmonic source modeling method," IEEE EPEC Electrical Power & Energy Conference 2009, Vol. 1, pp. 36-40.
[52] W. Wang, E. E. Nino, W. Xu, "Harmonic impedance measurement using a thyristor-controlled short circuit," IET Gener. Transm. Distrib. (2007), Vol. 1, N. 5, pp. 707-713.
[53] R. Langella, A. Testa, "A new method for statistical assessment of the system harmonic impedance and of the background voltage distortion" PMAPS International Conference on Probabilistic Methods Applied to Power Systems, June 2006, Vol. 1, pp.21-27.
[54] The INSPEC database is administered by the Institution of Electrical Engineerings. It was accessed through the AXIOM online research service (http://axiom.iop.org/) as subscribed to by Chalmers University of Technology.
[55] The IEEE standard dictionary of electrical and electronics terms, 6th ed., IEEE Std. 100-1996.
[56] Electromagnetic compatibility (EMC), Part 4, Section 30.
[57] J. Arrillaga, M. H. J. Bollen, and N. R. Watson. Power quality following deregulation. Proceedings IEEE, 88(2): 46–261, February, 2000.
[58] K. Bhattacharya, M. H. J. Bollen, and J. E. Daalder. Operation of Restructured Power Systems, Kluwer Academic, Boston, 2001.
[59] A. Woyte. Design issues of photovoltaic systems and their grid interaction. PhD thesis, Department Electrical Engineering, Katholieke Universiteit Leuven, Leuven, Belgium, December 2003.
[60] K. Macken. Analysis and control of renewable generation units used to improve power quality. PhD thesis, Department Electrical Engineering, November 2003, Leuven, Belgium, Katholieke Universiteit Leuven.
[61] N. Jenkins, R. Allan, P. Crossley, D. Kirschen, and G. Strbac. Embedded Generation. Institution of Electrical Engineers, London, 2000.
[62] R. C. Dugan, M. F. McGranaghan, S. Santosa, and H. W. Beaty. Electric Power Systems Quality, 2nd ed. McGraw-Hill, New York, 2003.
[63] A. Ghosh and G. Ledwich. Power Quality Enhancement Using Custom Power Devices. Kluwer Academic, Boston, 2002.
[64] Sharmistha Bhattacharyya and Sjef Cobben, "*Consequences of Poor Power Quality – An Overview,*" Technical University of Eindhoven,The Netherlands
[65] "Voltage Disturbances Standard EN 50160 - Voltage Characteristics in Public Distribution Systems," H. Markiewicz & A. Klajn, Wroclaw University of Technology. July 2004
[66] Keulenaer, H. De. (2003). "*The hidden cost of poor power quality,*" Leonardo Energy, European Copper Institute, October 2003. Available: www.leonardo-energy.org
[67] Manson, J.; Targosz, R. (2008). "*European power quality survey report,*" Leonardo Energy, November 2008, www.leonardo-energy.org.
[68] Lineweber, D. ; McNulty, S.R. (2001). "*The cost of power disturbances to industrial & digital economy companies,*" EPRI IntelliGrid Initiative (A Primen report from EPRI & CEIDS), Ref no. 1006274, June 2001. Available : www.epri.com/ceids

[69] CEER (2008). 4th Benchmarking report on quality of electricity supply 2008. Issued by: Council of European Regulators ASBL, Brussels, December 2008. Ref.: C08-EQS-24-04.